

# Experimental and numerical investigations on axial crushing of square cross-sections tube with vertical wave

Arameh Eyvazian<sup>1</sup>, Elsadig Eltai<sup>1</sup>, Farayi Musharavati<sup>1</sup>, Hossein Taghipoor<sup>2</sup>,  
T.A. Sebaey<sup>3,4</sup> and Pouyan Talebizadehsardari<sup>\*5,6</sup>

<sup>1</sup>Mechanical and Industrial Engineering Department, College of Engineering, Qatar University, P.O. Box 2713, Doha, Qatar

<sup>2</sup>Department of Mechanical Engineering, Velayat University, P.O. Box 99111-31311, Iranshahr, Iran

<sup>3</sup>Engineering Management Department, College of Engineering, Prince Sultan University, Riyadh, Saudi Arabia

<sup>4</sup>Mechanical Design and Production Department, Zagazig University, P.O. Box 44519, Zagazig, Sharkia, Egypt

<sup>5</sup>Metamaterials for Mechanical, Biomechanical and Multiphysical Applications Research Group,

Ton Duc Thang University, Ho Chi Minh City, Vietnam

<sup>6</sup>Faculty of Applied Sciences, Ton Duc Thang University, Ho Chi Minh City, Vietnam

(Received October 29, 2019, Revised May 6, 2020, Accepted June 24, 2020)

**Abstract.** In this paper, wavy square absorbers were experimentally and numerically investigated. Numerical simulations were performed with LS-Dyna software on 36 wavy absorbers and their crushing properties were extracted and compared with the simple one. The effect of different parameters, including wave height, wave depth, and wave type; either internal or external on the crushing characteristics were also investigated. To experimentally create corrugation to validate the numerical results, a set of steel mandrel and matrix along with press machines were used. Since the initial specimens were brittle, they were subjected to heat treatment and annealing to gain the required ductility for forming with mandrel and matrix. The annealing of aluminum shells resulted in a 76% increase in ultimate strain and a 60% and 56% decrease in yield and ultimate stresses, respectively. The results showed that with increasing half-wave height in wavy square absorbers, the maximum force was first reduced and then increased. It was also found that in the specimen with constant diameter and half-wave depth, an increment in the half-wave height led to an initial increase in efficiency, followed by a decline. According to the conducted investigations, the low maximum force can be observed in the specimen with zero half-wave depth as compared to those having a depth of 1 cm.

**Keywords:** axial compression; buckling; energy dissipation; quasi-static; numerical analysis

## 1. Introduction

Energy absorbers have been widely used to enhance the safety of motor vehicles such as cars and trains. These structures can be categorized as reversible and irreversible. The thin-walled structures are classified as irreversible absorbers. These absorbers reduce the damage and injuries to the body and occupants of vehicles by absorbing the kinetic energy of an accident and converting it into plastic deformation. Numerous researchers are searching for absorbers capable of declining the damages as much as possible. Transport engineers consider different parameters for the optimal design of energy absorbers, some of which are discussed below. The first parameter is the specific energy absorption (SEA) defined as the ratio of the energy absorbed by the absorber to its mass. Another important parameter that should be taken into account is the maximum crushing force ( $F_m$ ) usually appearing in the early phases of the crushing process. The next important parameter is the average crushing force ( $F_a$ ). The crush force efficiency (CFE) can be obtained by dividing the average crushing force ( $F_a$ ) to the maximum crushing force ( $F_m$ ). Volume

efficiency and crush efficiency are among the other parameters defined for energy absorbers. An optimum absorber is the one with high specific energy absorption, low maximum force, and high crush force efficiency.

Energy absorbers can be made with a variety of cross-sections (Bigdeli and Damghani Nouri 2019). The thin-walled square shells have been extensively used in various industries due to their high efficiency. In the following, some studies regarding the theoretical and analytical investigation of these absorbers are reviewed.

Wierzbicki and Abramowicz (1983) examined the folding of thin-walled columns with polygon cross-section under axial loading. By equating the work done by the external axial force on a square column to the internal dissipated energy by the column they obtained an average folding force for a square column. In another study (Abramowicz and Wierzbicki 1989), they rewrote and modified a complex theory to predict the behavior of polygonal columns by introducing axially-loading compression corner elements. Abramowicz (1983) also explored the theory of effective folding distance in the thin-walled columns. Comparing his results with previous which were often based on the assumption of completely plastic material, he considered the effect of strain hardening in his calculations. In another study by Abramowicz and Jones, the average folding force for asymmetric compression in

\*Corresponding author, Ph.D.  
E-mail: ptsardari@tdtu.edu.vn

square tubes was calculated (1984).

Hayduk and Wierzbicki (1984) studied the crushing state and deformation expansion in the square thin-walled elements. They theoretically calculated the upper and lower bounds for the average crushing force in the cross-shaped structures under bending and tensile deformation and concluded that the expansion deformations are less probable during the crushing compared to non-expansion deformations. In another study, Abramowicz (2003) investigated the square thin-walled structure as an energy absorber based on the superfolding element theory. He theoretically predicted the effective folding distance in metal thin-walled square columns under the axial compression and found that the effective folding distance of the square columns is about 70% of its original height for a column without reinforcement, and about 60% of its original height for the column with horizontal reinforcement, which was in good agreement with the experimental results. Zhao and Abdennadher (2004) evaluated their theory on an ideal square column and provided an acceptable prediction of the maximum crushing force in both quasi-static and dynamic loading states. They reported higher tensile strains on the edges of the thin-walled rectangular wall under the impact load due to the inertia; moreover, they found an ascending trend in the initial crushing force to enter the plastic region with loading. Ye *et al.* (2007) investigated the mechanism of plastic deformation in square and triangular columns under axial compressive loading. In the constructed columns, steel circular pipes with a yield stress of 1350 MPa were welded to each corner of the thin-walled column. Najafi and Rais-Rohani (2011) examined the energy absorption and axial folding in square thin-walled columns and offered a relation to calculate the average crushing force of these columns by considering the plastic kinetic crushing strength of the polygonal columns. In this theoretical model, the isotropic materials were described as perfect rigid-plastic materials, and the total internal energy was calculated taking into account the bending and axial deformation of the members during the crushing process. Niknejad *et al.* (2010) theoretically calculated the instantaneous crushing force of basic folding elements and square columns. For this purpose, they calculated the dissipated energy rate due to tensile and bending force around the horizontal and inclined hinges, and equated them to the external work applied to the square column; eventually, they calculated the instantaneous force for deformation of the basic folding mechanism (BFM).

Recently, Damghani *et al.* (2016b, 2017, 2019b) conducted a numerical and experimental study on the energy absorption by aluminum foam and corrugated core sandwich panel structures using the drop hammer test. They improved the performance of the corrugated sandwich panel under dynamic load (2019a). Moreover, they analytically investigated the behavior of the sandwich structures (2011, 2016a, 2019c). Zargar *et al.* (2018, 2019, 2017) proposed improved conceptual modeling in which the beams and panels of the structure were considered simplified beam elements. They also explored the advantage of this conceptual modeling in determining the resonant

frequencies/mode-shapes in the case of a wheelhouse.

In this section, some of the researches regarding the analytical investigations of the solid rectangular thin-walled columns are presented. Reid *et al.* (1986) analyzed the dynamic and static axial crushing of square columns filled with foams of different densities; additionally, they investigated the interaction between filler foam and square steel column. Abramowicz and Wierzbicki (1988) also examined the folding of square columns filled with foam considering the foam-column interaction. They extended the previous analyses for thin-walled square column and calculated the effects of energy absorption of the foam within these columns. Furthermore, Santosa and Wierzbicki (1998) determined the mean force of the square columns filled with aluminum foam, taking into account the foam-column interactions. Song *et al.* (2005) studied the theory of square columns filled with aluminum foam to calculate the energy absorbed by aluminum foam considering foam volumetric variation, as well as the interactions occurring between the aluminum foam and the single cap and double cap columns. In a theoretical study by Wang *et al.* (2007), the dynamic and static mean force along with and interaction force were evaluated for single-cap and double-cap square columns filled with aluminum foam. Xiong and Gengdong (2007) assessed the energy absorption of square columns filled with aluminum foam and multi-cell square columns, both theoretically and numerically. Their results showed that the energy absorption of multi-cell columns was 50 to 100 times more than the foam-filled columns. Niknejad *et al.* (2011) theoretically studied the instantaneous force of square and rectangular columns filled with polyurethane foam under the axial compressive loading and calculated the instantaneous force of the foam-filled square columns which showed proper agreement with the experimental results.

Some experimental investigations regarding the square cross-section thin-walled structures are mentioned in the following. Hanssen *et al.* (2000) experimentally analyzed the foam-filled square thin-walled hollow columns of aluminum under dynamic and static loading. Based on the experimental observations, an empirical relationship was established between the folding force and energy absorption in these structures.

In another study (2001), they developed an optimal energy absorption scheme for aluminum square columns filled with aluminum foam. Reyes *et al.* (2004) studied the behavior of hollow and aluminum foam-filled thin-walled aluminum square columns under oblique loading and found that an increase in the loading angle relative to the axial direction will decrease the energy absorption compared to the axial loading. Their experimental studies also showed that high-density aluminum foam filler will significantly enhance the energy absorption capacity; however, the energy absorption per mass unit (specific energy absorption) was reduced compared to the hollow column. Shahbeyk *et al.* (2007) experimentally and numerically investigated the square columns filled with aluminum foam by creating a crushing path on the body of the thin-walled column under axial loading. Zarei and Kroger (2008) optimized the foam-

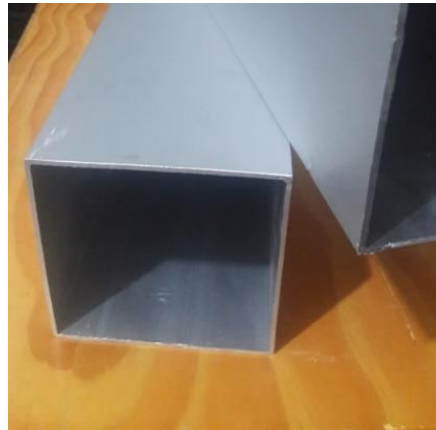


Fig. 1 Aluminum shells produced by extrusion absorbers some of which will be reviewed.

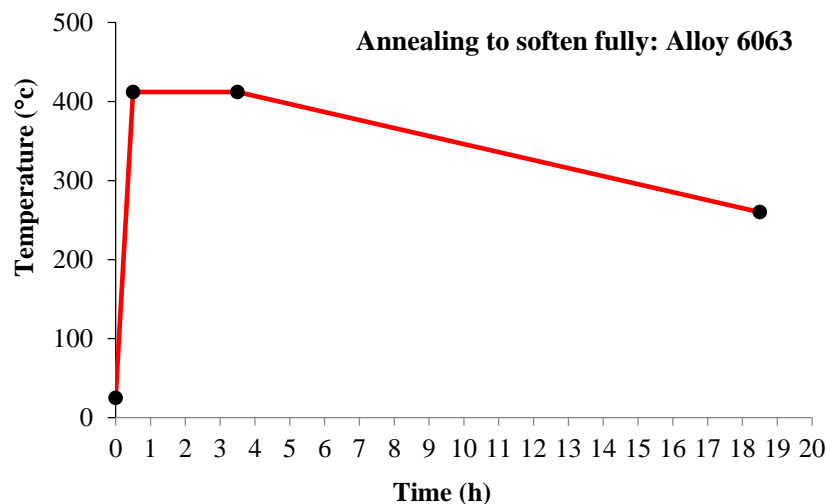


Fig. 2 Heating and cooling processes of aluminum shells to enhance their ductility and prevent rupture during the forming and crushing processes (Reynolds Metals 1958)

filled square hollow columns through geometrical optimization of the column to reach the highest energy absorption capacity at the lightest structure weight. Moreover, in another research (2008), they evaluated the folding phenomenon in square aluminum columns under axial and oblique impact loading and found that filling the columns is generally preferred to thicken the cylinder wall for augmenting the energy absorption performance. Zhang *et al.* (2009) examined the energy absorption of axial crushing for square columns with a buckling trigger lever at different heights in the column wall. Their results suggested that the average force and folding type did not change upon the utilization of buckling trigger lever, while the initial maximum force was reduced. In another experimental study on the square hollow and aluminum foam-filled thin-walled columns by Zhang *et al.* (2010), the higher energy absorption and deformation were reported in longitudinal compared to the transverse direction.

The application of wavy energy absorbers is one of the approaches to improve the crash boxes. In this regard, numerous studies have been conducted on wavy energy

Kılıçaslan (2015) numerically applied the aluminum foam-filling method to corrugated tubes to present a novel structure with excellent energy absorption capacity. In his study, dynamic crushing simulations were performed on finite element software LS-DYNA at an impact velocity of 16.7 m/s (corresponding to 60 km/h). Wu *et al.* (2016) introduced a novel tubal configuration, namely a sinusoidal corrugation tube (SCT), to control the collapse mode, and minimized the IPCF and fluctuations. They also investigated the effects of wavelength, amplitude, thickness, and diameter of SCTs on the energy absorption and collapse mode. Alkhatib *et al.* (2017) numerically studied the collapse behavior of corrugated tapered tubes under axial loading. The tested structures were subjected to axial impact by a striker's mass restricted to translational motion along the structures' axes. The effect of CTT's geometric (corrugated tapered tubes geometry) features on different performance indicators, namely the initial peak force (PF), energy absorption (EA), mean crushing force (MF), and specific energy absorption (SEA) was also explored. Shu *et al.* (2018) analyzed the crashworthiness of two-layered



Fig. 3 Wire-cut specimens for tensile test and their positioning in the SANTAM machine (ASTM Standard E8/E8M-13a, 2013)

Table 1 Mechanical properties derived from stress-strain curves in Fig. 4

Properties	$E$ (GPa)	$\sigma_y$ (MPa)	$\sigma_U$ (MPa)	Fracture strain
<b>6063-Annealed</b>	70	182	243	0.17
<b>6063-Extruded</b>	71	72	106.5	0.3

corrugated sandwich panels under crushing loading and found that the symmetrically-arranged corrugated sandwich panel has better energy absorption characteristics, which is more than 17.17% at 6 mm displacement before densification stage compared to regularly-arranged. Mao *et al.* (2019) evaluated the axial crushing of ultra-light all-metallic truncated conical sandwich shells with corrugated cores and designed and fabricated novel ultra-light all-metallic truncated conical sandwich shells (TCSS) with corrugated cores using the molding process.

By reviewing the published papers, it was found that thin-walled wavy absorbers with square cross-sections have not been investigated so far. Therefore, this study is aimed to assess the effect of the half-wave on the collapse characteristics of square absorbers. To this end, half-waves were created in both internal and external forms at two depths: 0 and 1 cm. Besides, three cases were considered for half-wave height, one of which was the overall case that has not been addressed before.

## 2. Experimental test

Aluminum thin-walled shells were prepared with a square cross-section of  $10 * 10 \text{ cm}^2$  and a thickness of 2 mm (Fig. 1). The specimens were produced through the extrusion process with high strain hardening, so the samples were brittle. To enhance the ductility of these specimens,

they were subjected to heat treatment based on the standards presented in Reference (1958).

Fig. 2 depicts the temperature variation of the shells inside the furnace. As can be seen, the temperature of the aluminum shells was raised from room temperature to  $412^\circ \text{C}$  within 30 min and kept at that temperature for 3 hr; then, the specimens were cooled down to  $260^\circ \text{C}$  in 15 hr and then exposed to free air.

After enhancing the ductility of the specimens according to the ASTM E8-E9 standard (2013), the dumbbell-shaped specimens were cut from the shell using a wire cut. The samples were then subjected to a tensile test by a 15-Ton SANTAM test machine. Using the data obtained from this test (displacement-force curve in the tensile test), the true stress-strain curve for the alloy used in this study can be extracted.

The dumbbell-shaped specimens and their positioning in the SANTAM machine are depicted in Fig. 3 and the true stress-strain curves are provided in Fig. 4. The true stress-strain curves before and after the annealing process are represented in Figs. 4(a) and 4(b), respectively. It should be noted that extensometer was used for data collection to increase the accuracy and precise determination of Young's modulus.

Moreover, to ensure the validity of the stress-strain curves of the annealed specimens, two specimens were prepared and their tensile test was repeated. Table 1 lists the

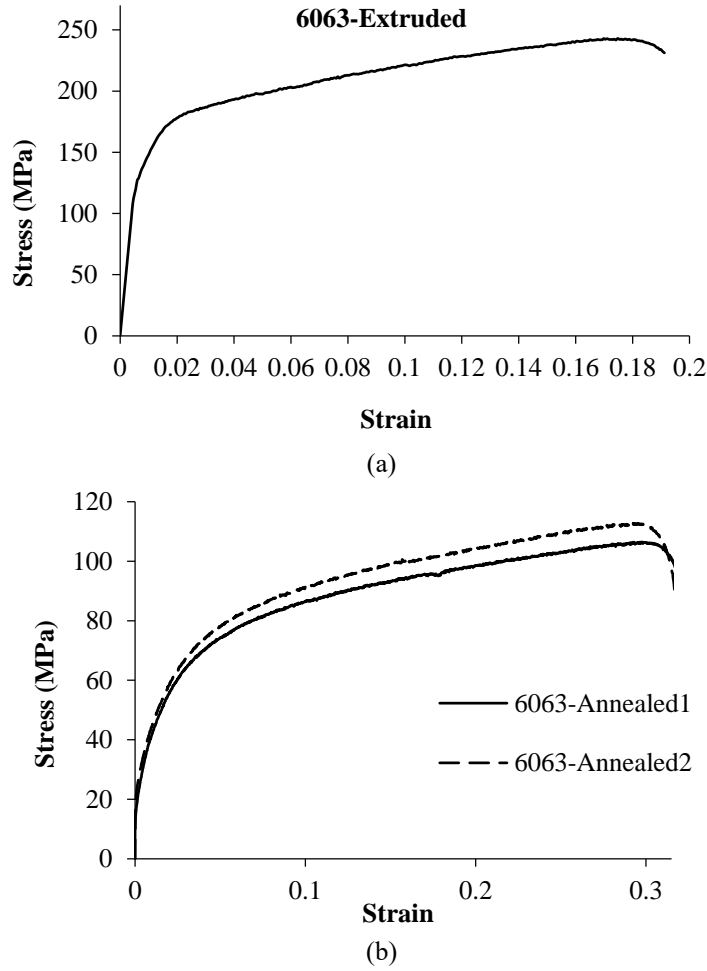


Fig. 4 True stress-strain curve (a) before the annealing process and (b) after the annealing process

mechanical properties derived from the stress-strain curves in Fig. 4.

### 2.1 Calculation of the important parameters in energy absorption

Initial peak force (PF), mean force (MF), energy absorption (EA), and crushing force efficiency (CFE) in addition to the specific energy absorption (SEA) were considered in measuring the absorber properties. Regarding the lower weight of the core compared to the top and bottom plates, the SEA was introduced to enhance the accuracy of topology optimization. Eqs. (1)-(4) (Taghipoor and Noori, 2018) represent the absorbed energy, initial peak force, crushing force efficiency, and the specific absorbed energy, respectively.

$$EA = \int_0^{\delta_{\max}} F(\delta) d\delta \quad (1)$$

$$MF = \frac{1}{\delta_{\max}} \int_0^{\delta_{\max}} F(\delta) d\delta \quad (2)$$

$$CFE = \frac{P_{\text{mean}}}{P_{\text{peak}}} \times 100 \quad (3)$$

$$SEA = \frac{E_a}{W} \quad (4)$$

Weight was considered as a limiting factor. The absorbed energy was defined as the area under the force-displacement curve. The crushing force efficiency can be obtained by dividing the mean force to the initial peak force (Taghipoor and Damghani Nouri 2018, 2019).

### 3. Simulations

Numerical simulations of this study were performed using LS-Dyna software. Side length, thickness, and height of all simulated absorbers were taken similar to those of the experimental samples (100, 2, and 200 mm, respectively). A simulated model is shown in Fig. 5. According to this figure, the energy absorbers were placed between the upper and lower jaws. The lower jaw was fixed, while the upper jaws could move downwards quasi-statically for 165 mm. Upper and lower jaws were considered rigid. Absorbers were

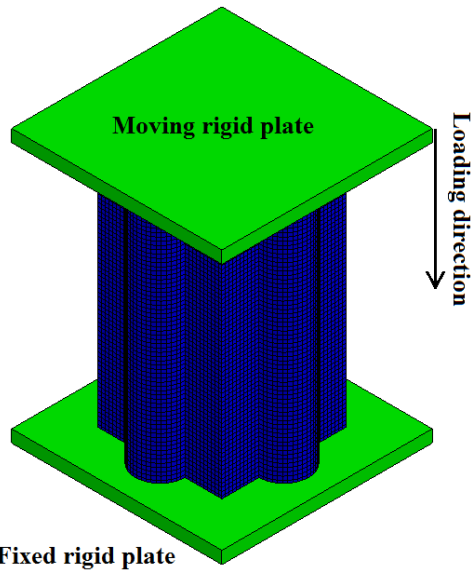


Fig. 5 Simulated finite element model in LS-Dyna software

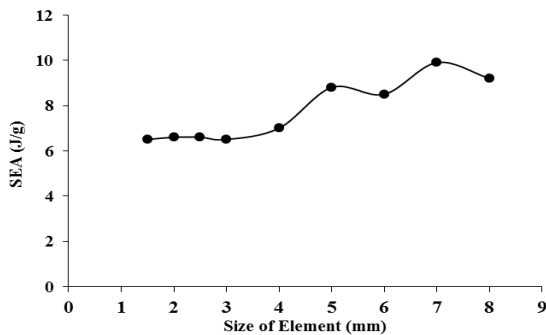
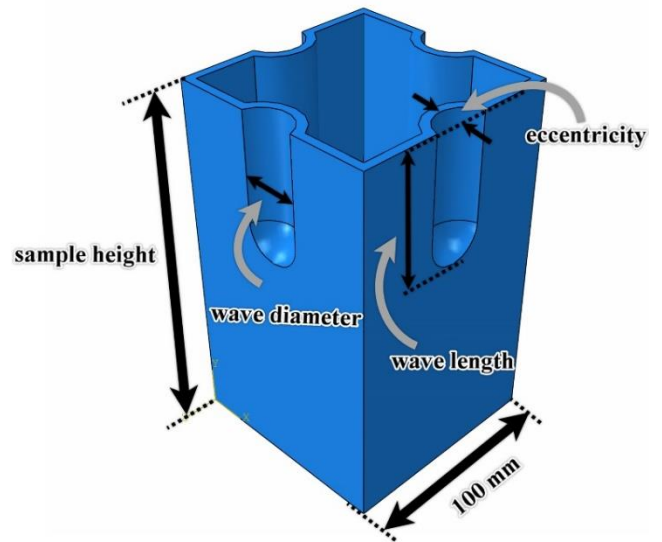
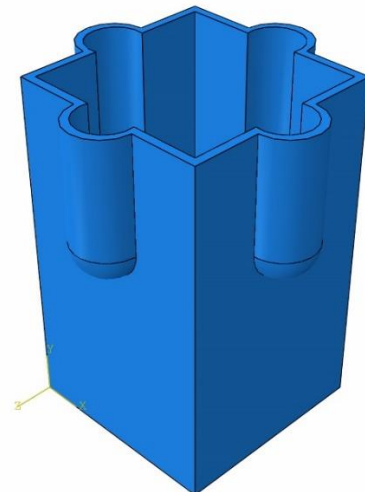


Fig. 6 Element convergence for a simple square absorber

simulated in the form of shells with approximate dimensions of  $3 \times 3 \text{ mm}^2$ . To obtain suitable dimensions for the elements, the specific energy parameter was considered for a simple absorber and this value was obtained with different elements. Specific energy variation in terms of the element dimensions is plotted in Fig. 6. As can be seen, by reducing the element dimension from 8 to 3, the convergence was improved, therefore, a square with the dimensions of  $3 \times 3 \text{ mm}^2$  was selected. It should be noted that a further decrease in elements dimensions may lead to an increase in computational time without any considerable improvement in the results. The specifications mentioned in Table 1 were imported for the annealed material in the mat-piecewise-linear-plasticity model in the LS-Dyna software. This model is suitable for simulating the behavior of metal energy absorbers as well as materials with linear stress curves in the plastic region. To define the interference between the jaws and absorber as well as the interference between the absorbing components, the static and dynamic coefficients were considered 0.3 and 0.2, respectively. These values are obtained after applying several different values, in order to achieve the greatest agreement between experimental and numerical results. CONTACT-



Internally waves



Externally waves

Fig. 7 Schematic of the parameters studied in the wavy square absorber

AUTOMATIC-SURFACE-TO-SURFACE and CONTACT-AUTOMATIC-SINGLE-SURFACE models are used for defining contact between the jaw elements with the sample elements and the sample elements with each other, respectively. CONTACT-AUTOMATIC-SURFACE-TO-SURFACE is a recommended contact type since, in crash simulations, the orientation of parts relative to each other cannot always be anticipated as the model undergoes large deformations.

### 3.1 Simulated samples

36 different wavy square absorbers were simulated in this research. The thickness, side length, and height of all samples were 2, 100, and 200 mm, respectively. The half-waves were simulated both internally and externally, with

Table 2 Collapse characteristics of simulated samples in the LS-Dyna software (the height of all samples is 20 cm)

Simple	Energy (J)	mass (g)	SEA (J/g)	PF (kN)	MF (kN)	CFE (%)
Simple	2775.2	430	6.5	50.4	16.8	33.4
I5.2.0	3413.6	445	7.7	46.4	20.7	44.6
I5.3.0	3823	453	8.4	43.8	23.2	53
I5.4.0	3846.9	463	8.3	39.7	23.3	58.7
I10.2.0	3022.9	457	6.6	44.9	18.3	40.8
I10.3.0	4223.4	472	8.9	41.3	25.6	62
I10.4.0	4818.5	488	9.9	38.5	29.2	75.8
I20.2.0	3945	479	8.2	62	23.9	38.6
I20.3.0	7080.3	504	14	68.7	42.9	62.4
I20.4.0	7839.6	528	14.8	73.4	47.5	64.7
I5.2.1	3881.4	471	8.2	47.3	23.5	49.7
I5.3.1	3850.7	482	8	44	23.3	53
I5.4.1	3254.3	494	6.6	44	19.7	44.8
I10.2.1	4683.8	504	9.3	46.3	28.4	61.3
I10.3.1	5055.6	522	9.7	45.5	30.6	67.3
I10.4.1	5183.4	540	9.6	40.4	31.4	77.7
I20.2.1	8009.4	565	14.2	75.9	48.5	64
I20.3.1	8531.6	590	14.5	81.2	51.7	63.7
I20.4.1	8822.6	614	14.4	85.1	53.5	62.9
O5.2.0	4174	445	9.4	45.2	25.3	56
O5.3.0	3731	453	8.2	43.1	22.6	52.4
O5.4.0	3617.7	463	7.8	40.8	21.9	53.7
O10.2.0	4024	457	8.8	45.2	24.4	54
O10.3.0	4322.5	472	9.2	42.7	26.2	61.4
O10.4.0	4701.4	488	9.6	40.1	28.5	71.1
O20.2.0	4972.7	479	10.4	60.2	30.1	50.1
O20.3.0	6684.9	504	13.3	65.1	40.5	62.2
O20.4.0	6591.5	528	12.5	68.1	39.9	58.6
O5.2.1	3711.6	471	7.9	48.2	22.5	46.7
O5.3.1	3654.8	482	7.6	51.7	22.2	42.9
O5.4.1	3877	494	7.8	44.2	23.5	53.2
O10.2.1	4490.6	504	8.9	47.5	27.2	57.3
O10.3.1	5603.7	522	10.7	46.2	34	73.6
O10.4.1	5149.1	540	9.5	42.1	31.2	74.1
O20.2.1	6248	565	11.1	73.3	37.9	51.7
O20.3.1	3810.5	590	6.5	77.2	23.1	29.9
O20.4.1	3763.9	614	6.1	79.6	22.8	28.6

three lengths of 5, 10, and 20 cm. Three diameters of 2, 3, and 4 cm were considered for the half-waves at two depths of 0 and 1 cm.

A combination of letters and numbers was used to label the simulated models. The first letter (O or I) represents the internal or external half-wave while the subsequent numbers are the indicator of half-wave lengths (5, 10, and 20 cm), half-wave diameter (2, 3, and 4 cm) and the eccentricity (0 and 1 cm).

For example, O20.4.1 implies a square wave absorber with an external wave with a diameter of 4 cm, length of 20 cm, and eccentricity of 1 cm on its walls. All the examined parameters are shown in Fig. 7. In Table 2, the crushing characteristics of 36 different models along with a simple specimen are illustrated. In the next section, the results will be validated.

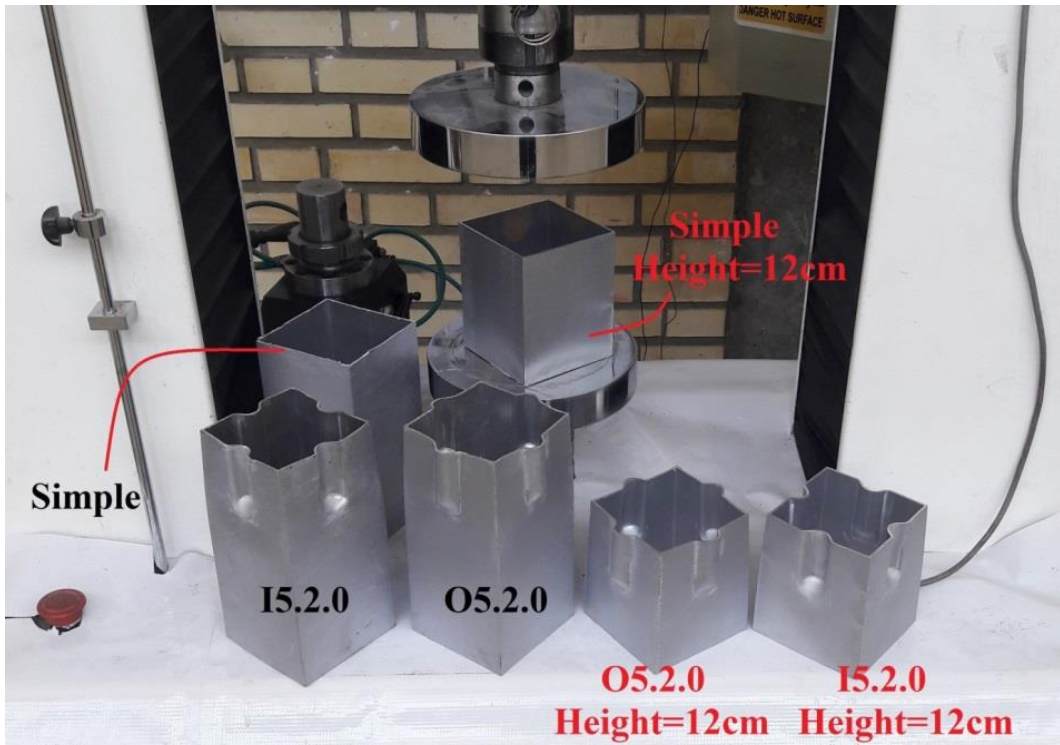


Fig. 8 Experimental specimens constructed for verification purposes

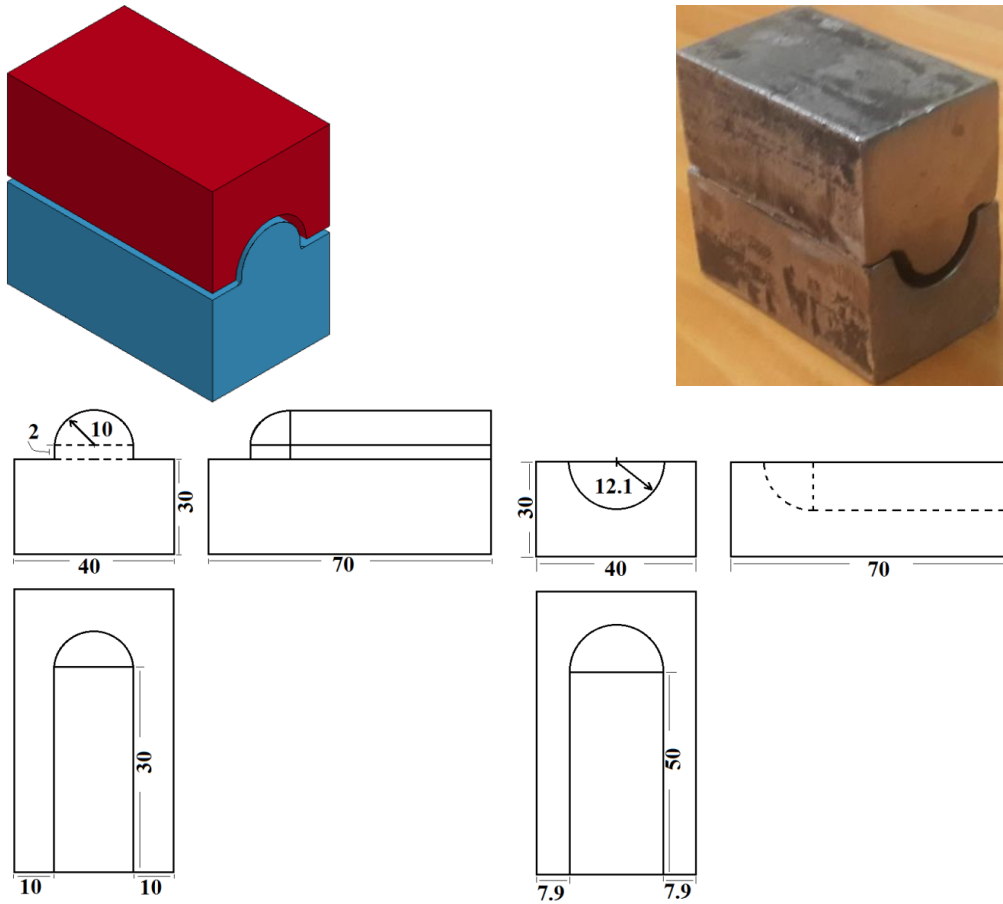


Fig. 9 Geometric dimensions of the mandrel and the matrix used to make wavy absorbers (dimensions are in mm).

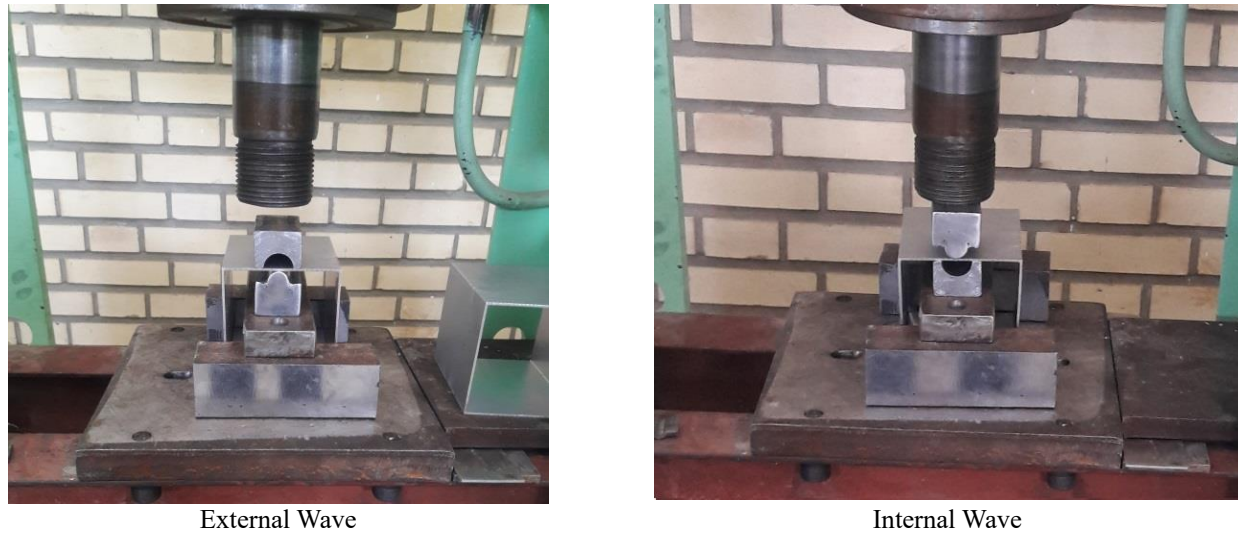


Fig. 10 The positioning of mandrel and matrix on the press for creating internal and external waves

Table 3 Experimental and numerical collapse specifications of the tested specimens for validation purposes

Specimen code	Energy (J)			$F_m$ (kN)			CFE (%)		
	E*	S**	D*** (%)	E	S	D	E	S	D (%)
Simple/20	2863	2775	-3.1	48.6	50.4	3.7	42.1	39.3	-6.5
I5.2.0/20	3506	3413.6	-2.6	44.0	46.4	5.5	46.6	44.6	-4.3
O5.2.0/20	4078	4174	2.3	42.8	45.2	5.6	59.1	56	-5.2
Simple/12	2232	2300	3.0	48.6	51.4	5.8	45.9	44.7	-2.6
I5.2.0/12	1210	1240	2.5	43.7	46.4	6.1	27.7	26.7	-3.5
O5.2.0/12	1377	1330	-3.4	45.8	47.2	3.0	30.1	28.2	-6.2

\*E $\equiv$ Experimental model,

\*\*S $\equiv$ Simulated model,

\*\*\*D $\equiv$ Difference between simulated model and Experimental model

### 3.2 Validation of the simulation results

To make sure of the accuracy and validity of the simulations, simple specimens of I5.2.0 and O5.2.0 were constructed at the height of 20 cm. Furthermore, to consider some variations in the experimental specimens, some of them were constructed with a height of 12 cm. Totally, 6 different cases were constructed as depicted in Fig. 8.

The simple specimen can be easily constructed, but to construct I5.2.0 and O5.2.0 specimens, a mandrel and matrix set was made. The geometric dimensions of the constructed matrix are provided in Fig. 9. As denoted in Fig. 10, these mandrels and matrix can produce the required internal and external waveforms on the body of the simple aluminum specimen during a deep drawing process when placed in the press apparatus.

Constructed specimens were positioned in the SANTAM machine and collapsed during a quasi-static compression process. The force-displacement curves and their collapsed states in both experimental and numerical cases are illustrated in Figs. 11 and 12, respectively. Fig. 13 also depicts the cross-section of a simple specimen with a

height of 20 cm. The collapse phases of the I5.2.0/H=20 cm specimen in the experimental test are revealed in Fig. 14. A comparison between the collapse properties in experimental and numerical modes is provided in Table 3.

According to Table 3, the initial maximum forces in simulated specimens are higher than the experimental ones. This discrepancy can be assigned to the integrity and lack of distortion in the specimens during the numerical simulation which can't be achieved experimentally. The distortion in experimental specimens declined the maximum force required for collapse. Table 3 and Figs. 10-12 suggest a good agreement between experimental and numerical results. Therefore, since the validity of the simulation results is proved, the obtained numerical results can be discussed.

## 4. Results and discussion

In this section, the results of numerical simulations and experimental tests are investigated. The results of Table 2 are provided in the form of diagrams to further clarify the obtained results.

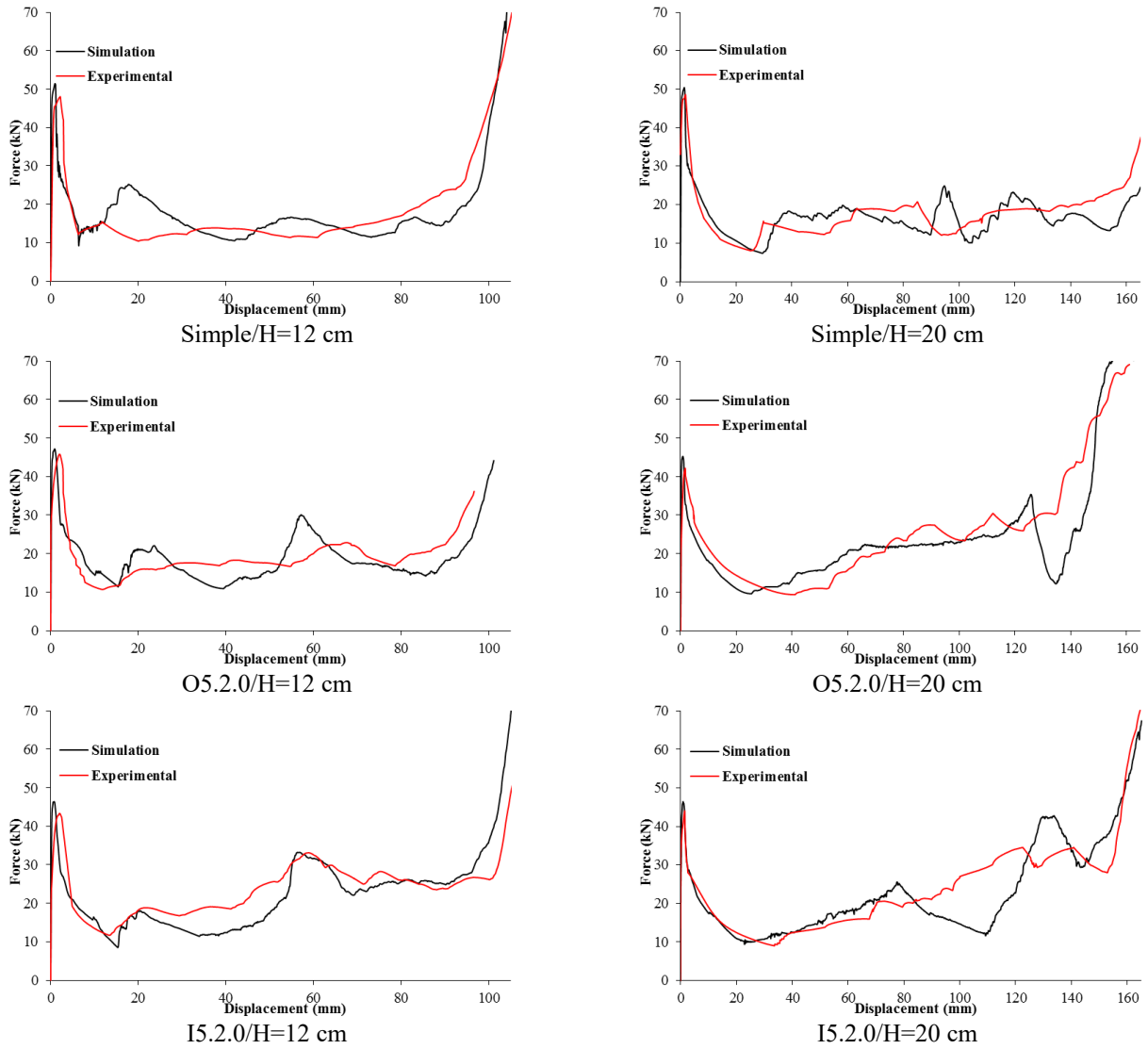
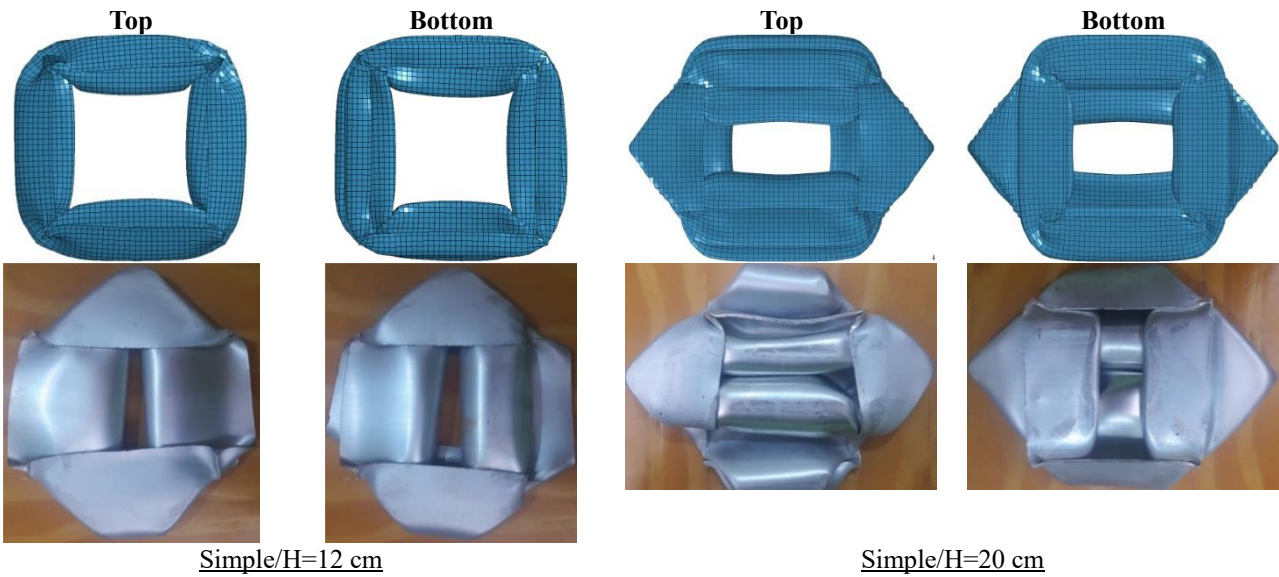


Fig. 11 The force-displacement curves of the constructed specimen of Fig. 8 in two experimental and numerical modes



Continued-

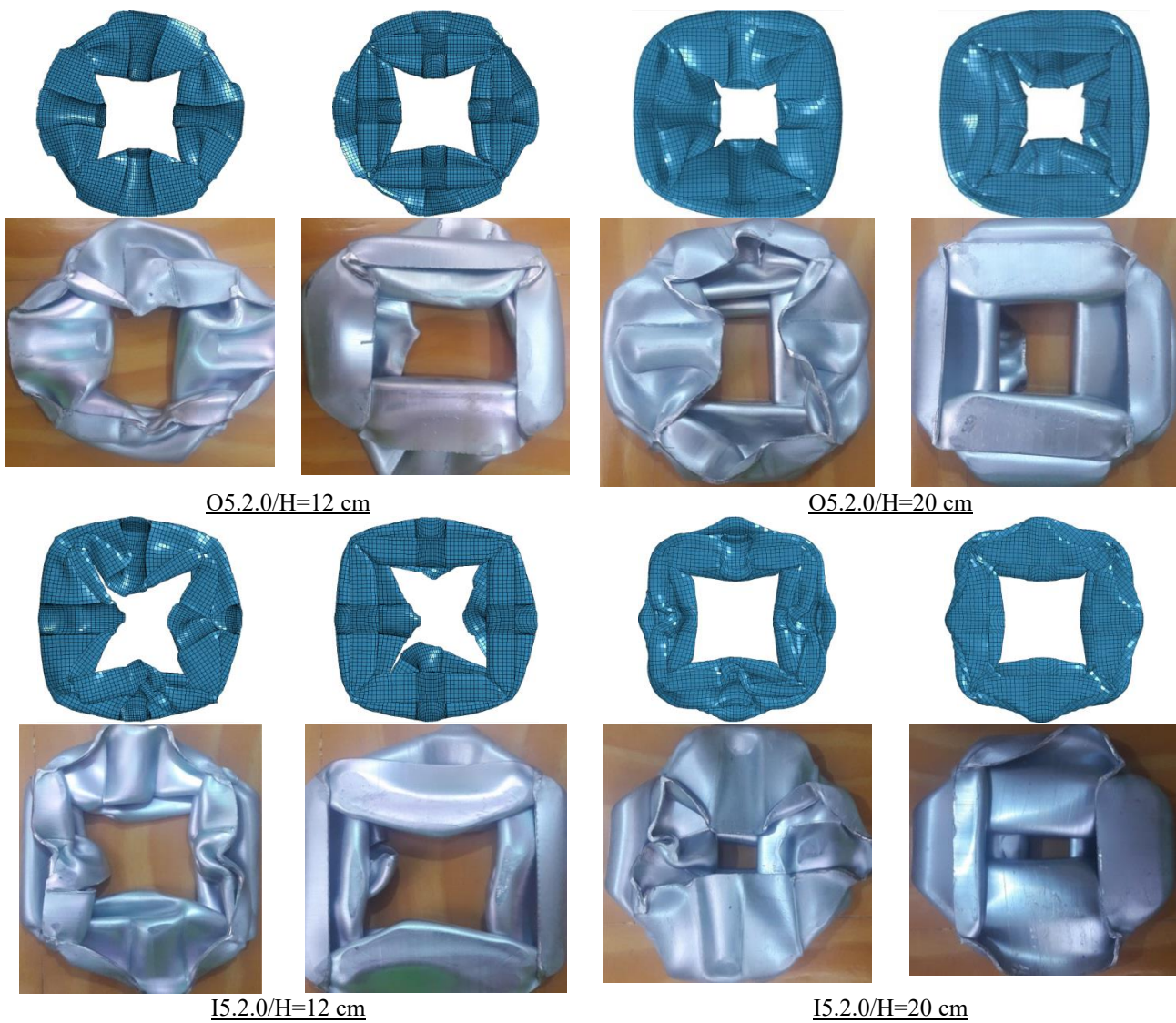


Fig. 12 Comparison of the experimental and numerical collapse states in the selected specimen for validation purposes

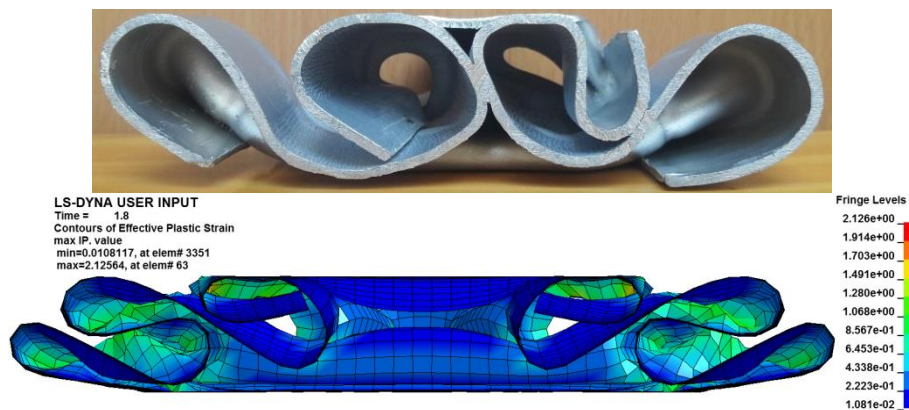


Fig. 13 The experimental and numerical cross-section of the simple specimen with a height of 20 cm

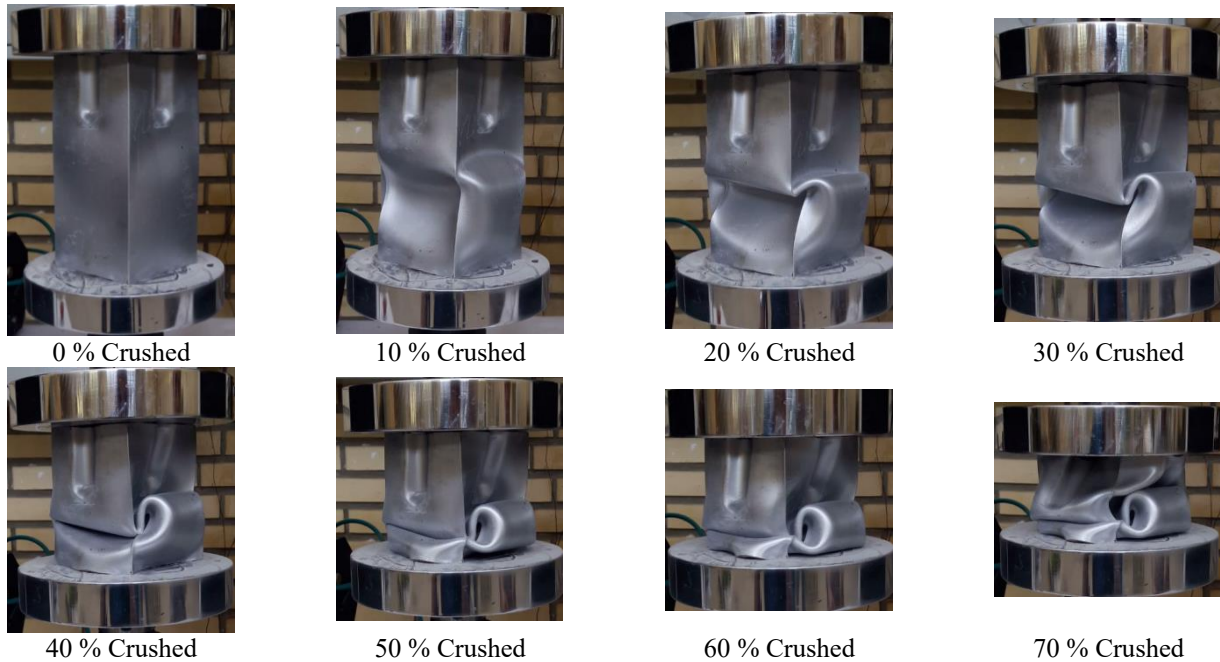


Fig. 14 The collapse phases of I5.2.0/H=20cm specimen in experimental mode

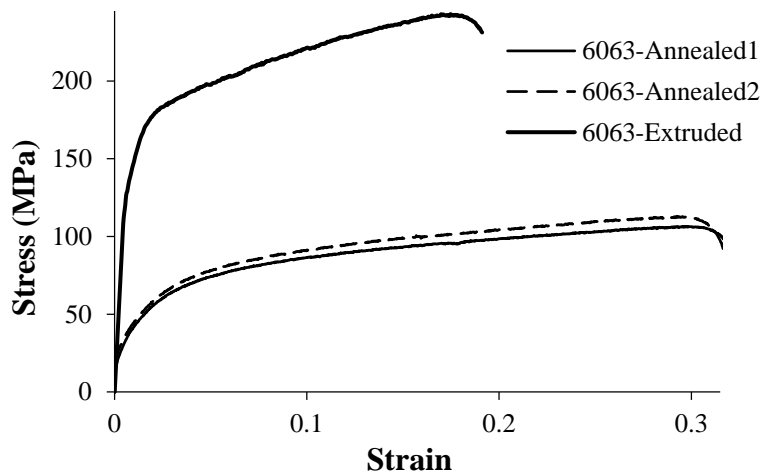


Fig. 15 True stress-strain curves of extruded specimens for the annealed and non-annealed cases

#### 4.1 Comparison of mechanical properties of annealed shell and normal shell

As already mentioned, the ductility of the aluminum shells was enhanced by heat treatment. In Fig. 15, the true stress-strain curves are compared in both extruded and annealed states. Moreover, the mechanical properties extracted from Fig. 15 are compared in Table 4.

According to the obtained results, the annealing process increased the ultimate strain by 76% along with 60% and 56% reduction in yield stress and ultimate stresses, respectively. It should be noted that the annealing process augmented the ductility of material during the formation of the wave. Wave creation in the non-annealed specimens may lead to an undesirable rupture phenomenon.

#### 4.2 Investigating the effect of half-wave diameter on energy absorption parameters

The results of Table 2 are depicted in Fig. 16. This figure plots the variation of crushing parameters as a function of the half-wave diameter.

According to the diagrams plotted for maximum force in samples with the half-wave height of 5 and 10 cm, an increase in the half-wave diameter led to a decline in the maximum force. However, in samples with a half-wave height of 20 cm, the increase in maximum force was followed by an increment in the half-wave diameter. Fig. 17 presents the force-displacement curves of O10.2.0, O10.3.0, O10.4.0, and simple (reference) specimens with a half-wave height of 10 cm. Fig. 18 also depicts the collapse phases of

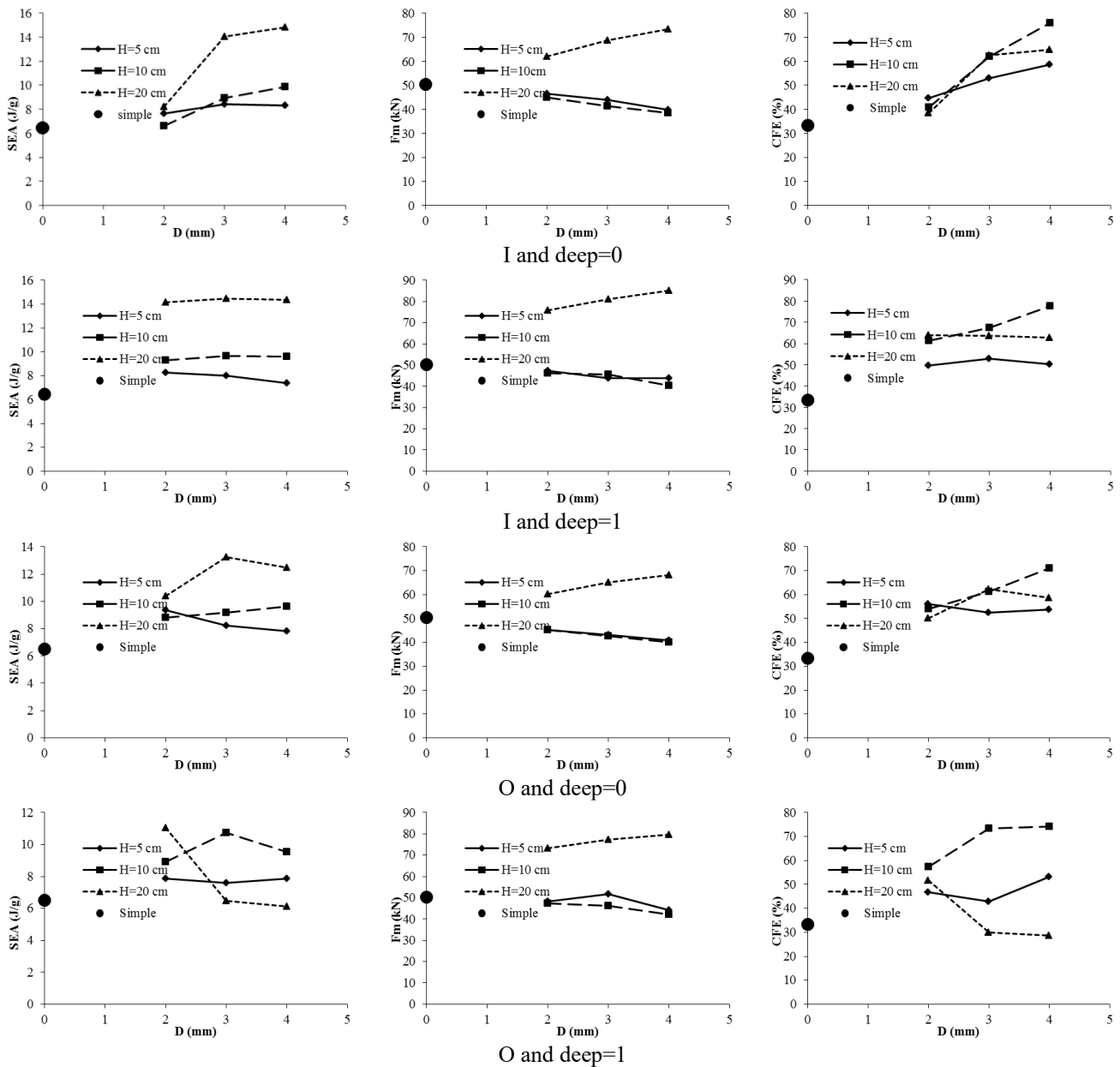


Fig. 16 The effect of the half-wave diameter on energy absorption parameters

Table 4 Comparison of mechanical properties of extruded specimens for both annealed and non-annealed cases

Properties	$E$ (GPa)	$\sigma_y$ (MPa)	$\sigma_U$ (MPa)	Fracture strain
<b>6063-Annealed</b>	70	182	243	0.17
<b>6063-Extruded</b>	71	72	106.5	0.3

I10.2.0, I10.3.0, and I10.4.0, as well as simple specimen, at the early phases of collapse.

The formation of curvature in the wall of the simple specimens led to a decrease in the initial maximum force. Fig. 19 provides the force-displacement diagram of I20.2.0, I20.3.0, I20.4.0, and simple specimens. The collapse phases of these specimens are also observed in Fig. 20 at the early

phases of the collapse. According to Fig. 20, the maximum Von Mises stress occurred in the specimen with the maximum half-wave diameter (I20.4.0 specimens).

Based on Fig. 16, the crushing force efficiency of the specimens with overall half-wave superseded the simple specimens, as well as those without overall half-waves.

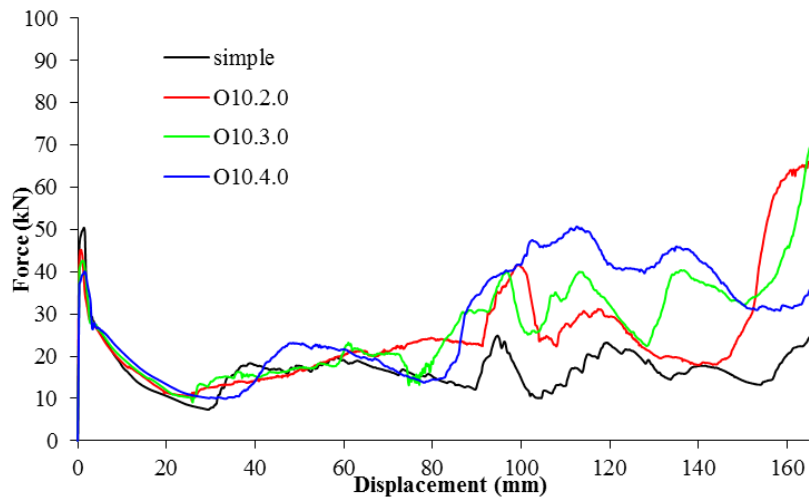


Fig. 17 Comparison of the force-displacement curve of O10.2.0, O10.3.0, O10.4.0, and simple specimens

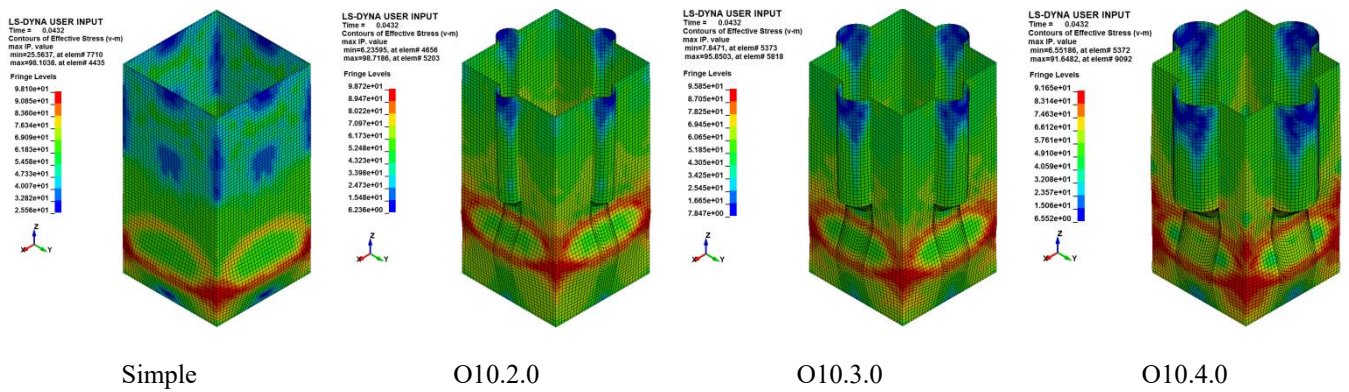


Fig. 18 The collapse mode of O10.2.0, O10.3.0, O10.4.0, and simple specimens in the early phases of the collapse process

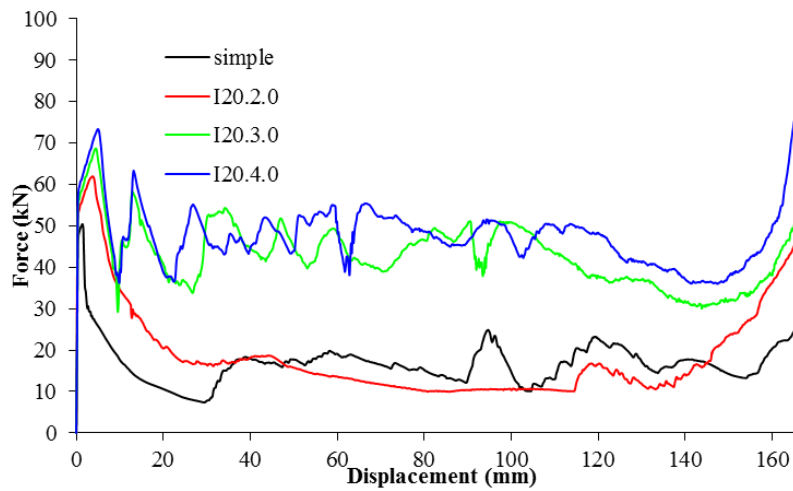


Fig. 19 The force-displacement curve of I20.2.0, I20.3.0, I20.4.0, and simple specimens

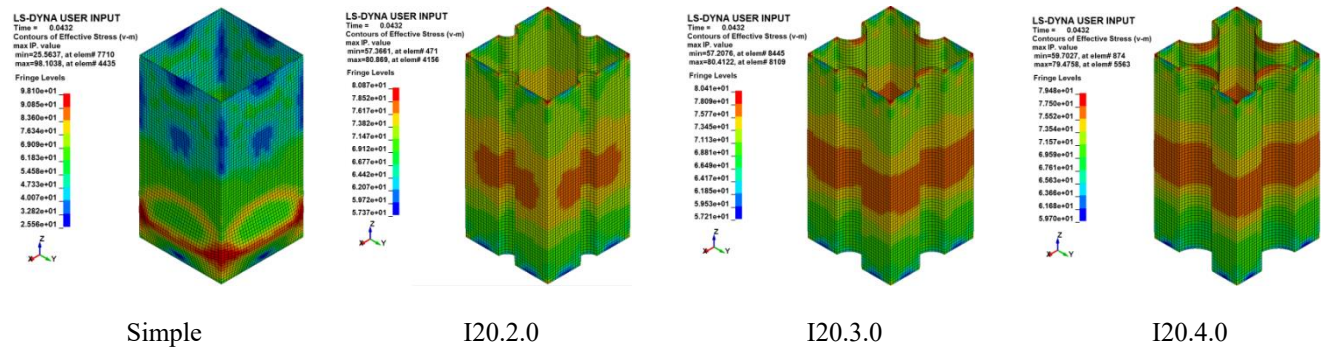


Fig. 20 The collapse mode of I20.2.0, I20.3.0, I20.4.0, and simple specimens

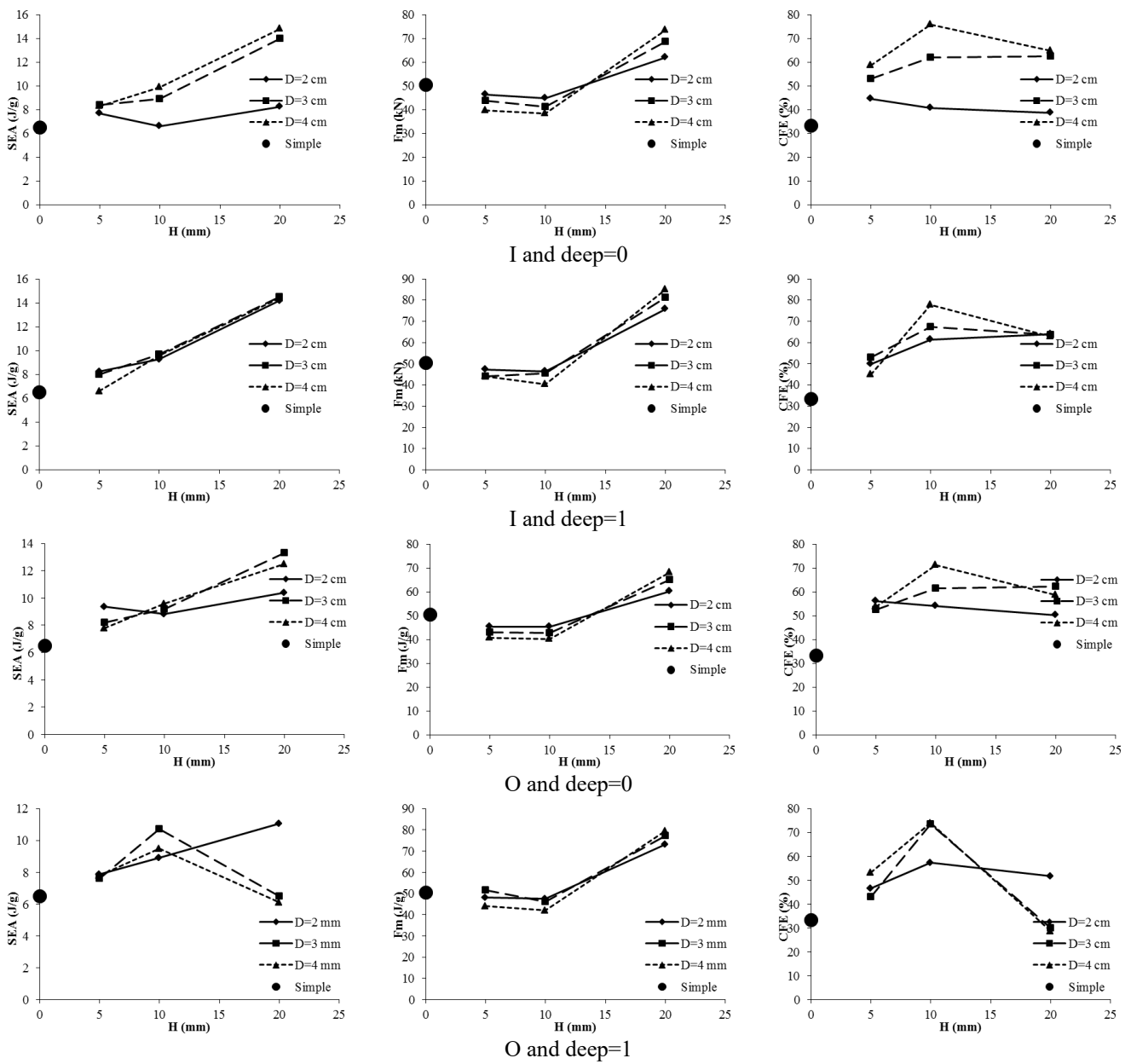


Fig. 21 Variation of energy absorption parameters in terms of half-wave height

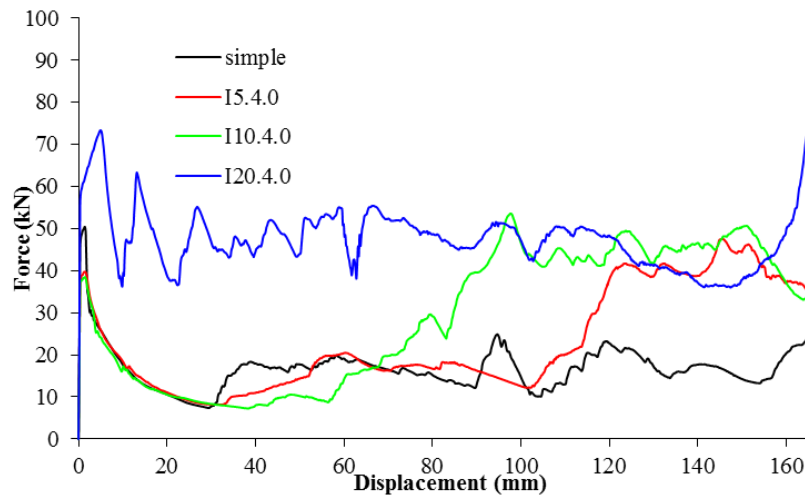


Fig. 22 Force-displacement diagrams for I5.4.0, I10.4.0, I20.4.0, and simple specimens

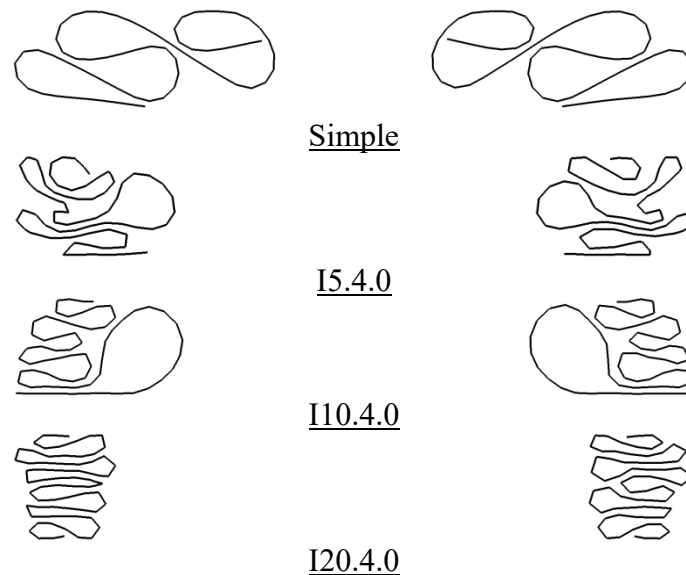


Fig. 23 Cross-section of I5.4.0, I10.4.0, I20.4.0, and simple specimen

#### 4.3 Effect of half-wave height on energy absorption parameters

Fig. 21 illustrates the effect of the half-wave height on the crushing characteristics derived from Table 2 data.

According to Fig. 21, in general, the energy absorption increased by the elevation of the half-wave height through changing the collapse pattern. If such changes lead to the creation of more folds, change of collapse pattern from symmetric to diamond, or provision of energy absorption through the inversion, the energy absorption will be increased. On the other hand, if the change in collapse pattern is accompanied by a decrease in the number of folds or symmetric folds, energy absorption will be reduced. Fig. 22 shows the force-displacement diagrams of I5.4.0, I10.4.0, I20.4.0, and simple specimens.

According to this figure, high energy absorption is observed for the I20.4.0 specimen. The greater energy absorption in the I20.4.0 specimen can be attributed to the greater plastic hinge in the collapse pattern of this specimen. The cross-section of I5.4.0, I10.4.0, I20.4.0, and simple specimens are shown in Fig. 23. Accordingly, the hinges formed in the I20.4.0 specimen are more than other specimens.

Concerning the maximum force, Fig. 21 suggests that in the wavy specimens, an increase in the half-wave height will reduce the maximum force followed by an increase. The collapsed phases of I5.4.0, I10.4.0, I20.4.0, and simple specimens in the early phases of collapse are also shown in Fig. 24.

Regarding the CFE diagrams of Fig. 21, in most cases, particularly in the specimens with greater half-wave lengths, the crushing force is higher than the simple ones.

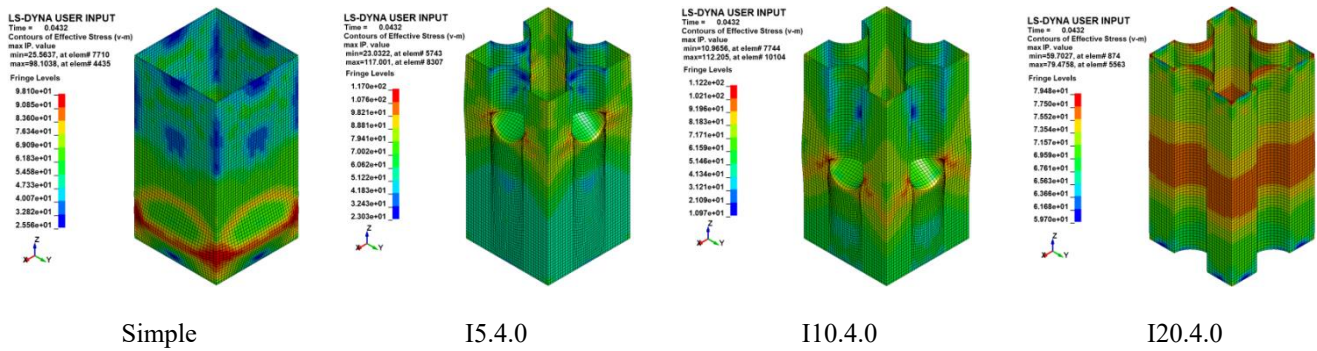


Fig. 24 Collapsed phases of I5.4.0, I10.4.0, I20.4.0, and specimens at the first 5 mm of collapse

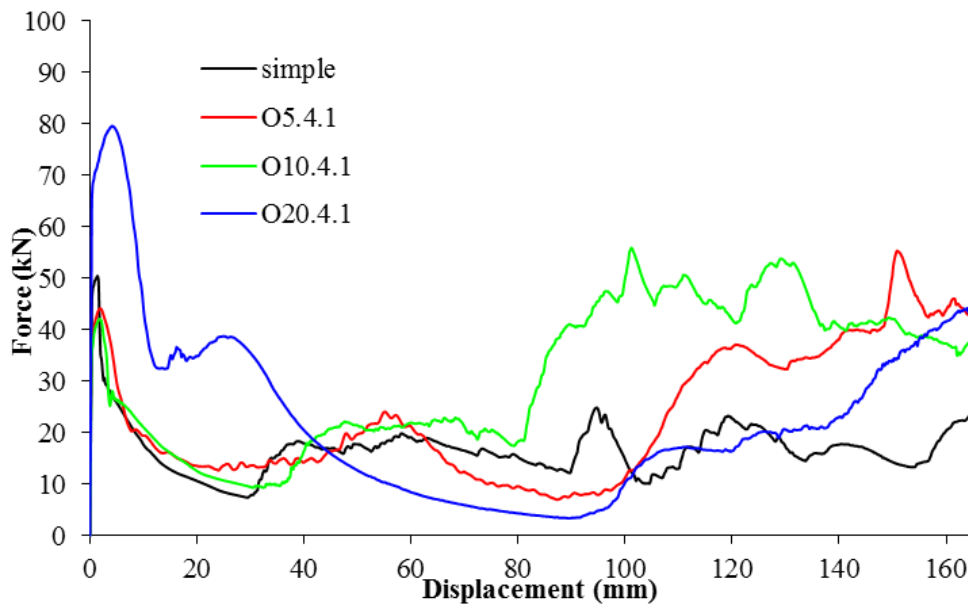


Fig. 25 Force-displacement diagram of O5.4.1, O10.4.1, O20.4.1, and simple specimens

According to Fig. 21, at constant diameter and depth of the half-wave, an increment in the height of the half-wave initially augmented the efficiency followed by a decrease. This figure declares that the highest efficiency is related to the specimen with a height of 10 cm. Fig. 25 shows the force-displacement diagram of O5.4.1, O10.4.1, O20.4.1, and simple specimens.

#### 4.4 Investigating the effect of half-wave depth on energy absorption parameters

As already mentioned, the waves were simulated in two depths. In the first case, the waves were half-circular with no depth, but in the second case, the waves became deeper for about 1 cm. Fig. 26 illustrates the effects of the half-wave depth on the collapse specification.

According to Fig. 26(a), the half-wave depth caused different impacts on energy absorption. A comparison of results with the horizontal line in Fig. 26(a) shows higher energy absorption in wavy specimens compared to the simple specimens.

Based on Fig. 26(b), the specimens with the half-wave depth of zero possessed smaller maximum force as compared to their peers with a depth of 1 cm. Similarly, Fig. 26(b) displays that the maximum force of the specimen with a half-wave height of 20 cm was greater than the simple ones; while the specimens with the half-wave height of 5 and 10 exhibited lower maximum forces (compared to the simple one). Fig. 27 shows the force-displacement curve of I20.3.0, I20.3.1, and simple specimens.

According to Fig. 26, the folding of the square specimens led to an increase in the crushing force in the majority of the cases. Furthermore, Fig. 26(d) suggests that specimens with a half-wave height of 10 cm and a depth of 0 have lower efficiency than those with a depth of 1 cm. The force-displacement curves of I10.2.0 and I10.2.1 specimen, along with the simple specimen, are demonstrated in Fig. 28. The collapse phases of I10.2.0 and I10.2.1 specimen are also shown in Figs. 29 and 30.

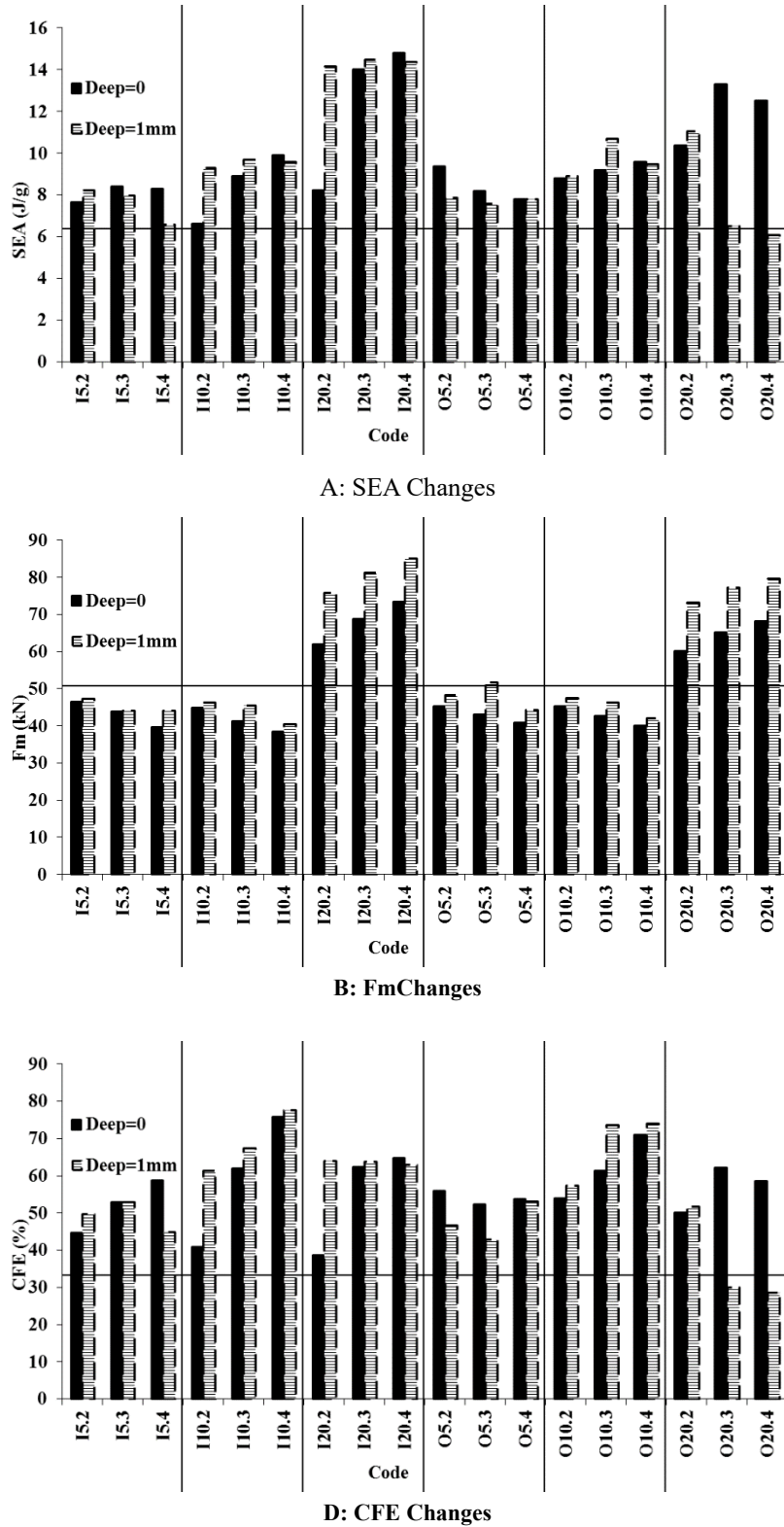


Fig. 26 Effects of half-wave depth on the collapse characteristics of the wavy absorbers

4.5 Investigation of the effect of internal and external half-waves on the energy absorption process

Fig. 31(a) shows that in the specimen with a wave

height of 20 cm, the internal wave led to more energy absorption as compared to the external wave. Moreover, Fig. 31(b) demonstrates that in the specimen with a wave height of 20 cm, the internal wave resulted in higher maximum

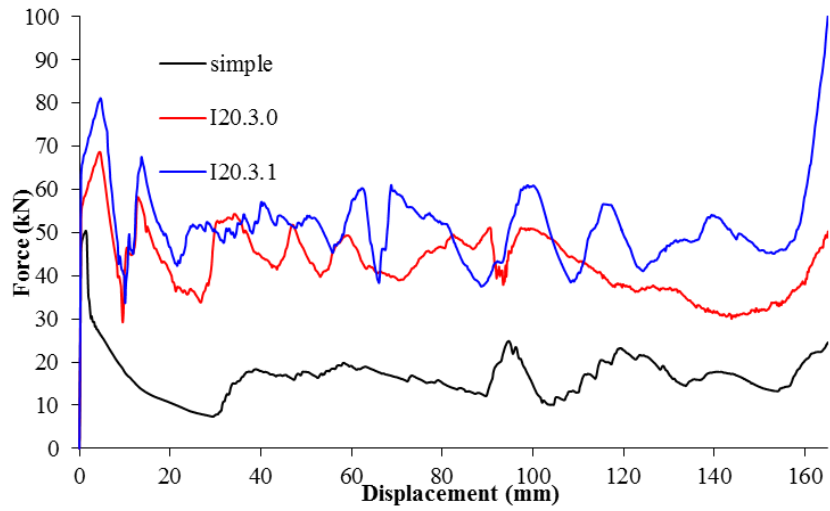


Fig. 27 Force-displacement diagram of I20.3.0 and I20.3.1 specimens along with the simple specimen

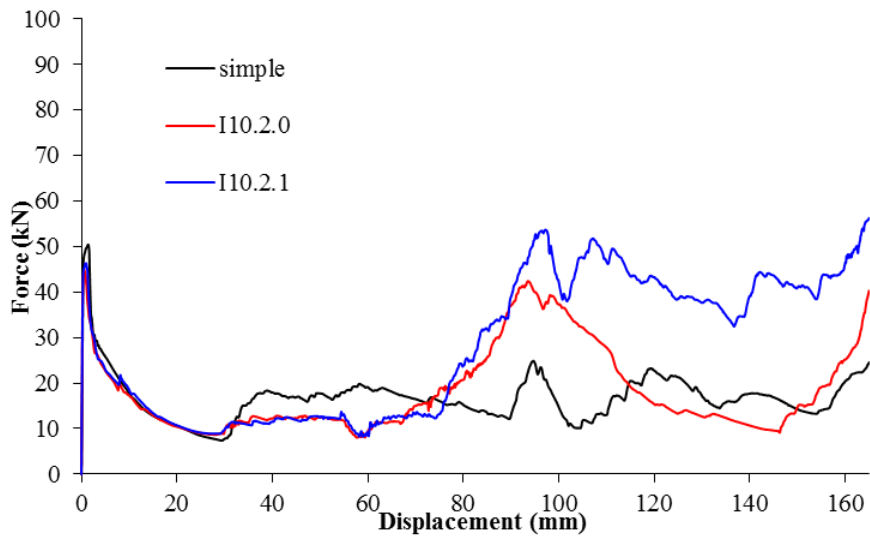
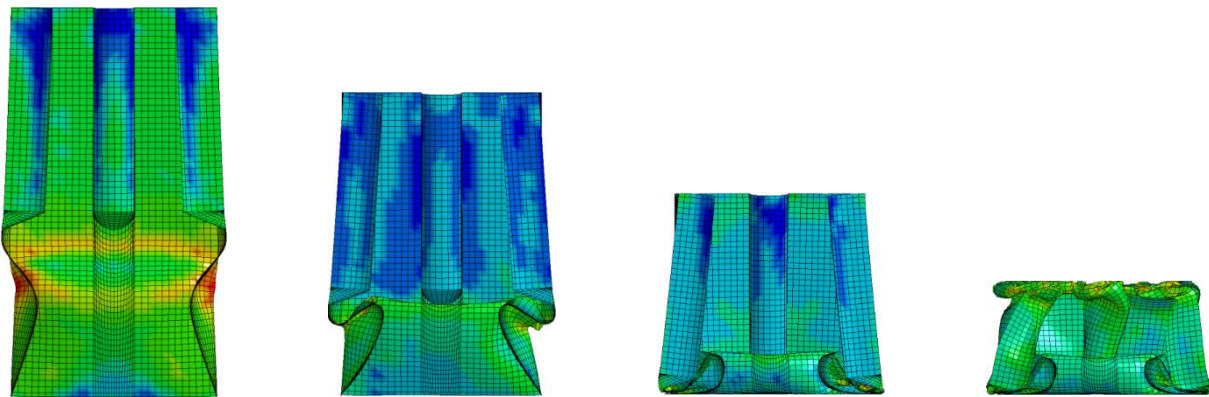


Fig. 28 Force-displacement diagram for I10.2.0 and I10.2.1 specimens along with the simple specimen



Continued-

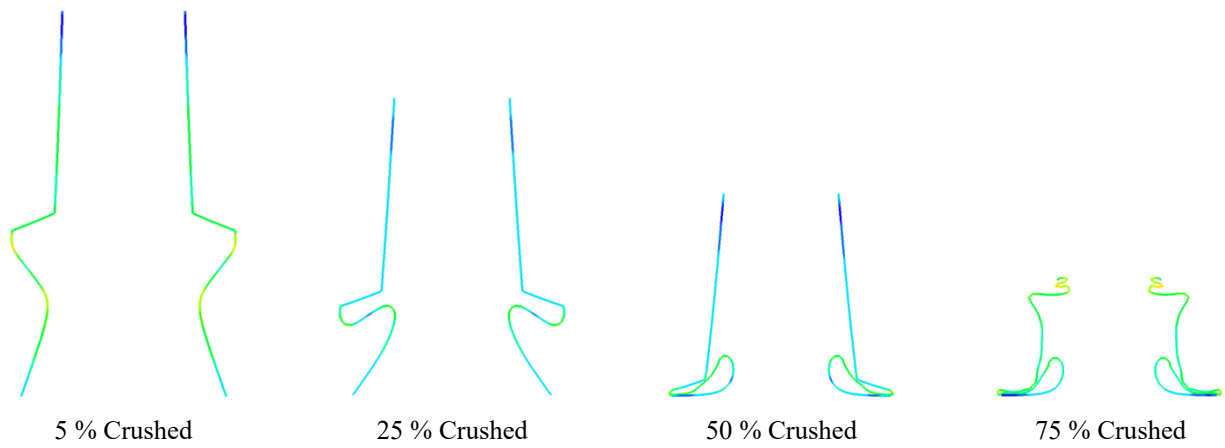


Fig. 29 Collapse phases of I10.2.0 specimen

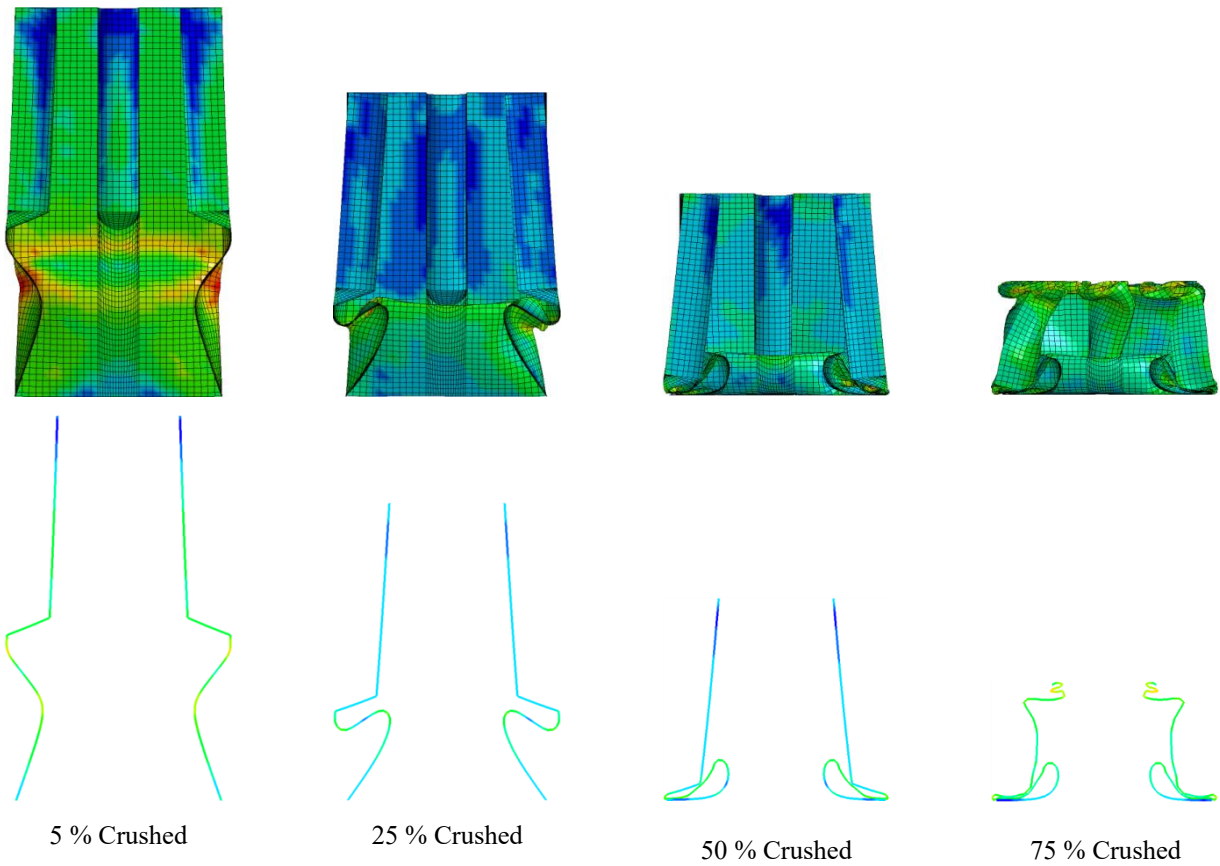


Fig. 30 Collapse phases of I10.2.1 specimen

force and efficiency than the external wave.

Fig. 32 presents the force-displacement curve of I20.3 Fig. 31(d) revealed that the specimens with a high half-wave diameters of 3 and 4 cm exhibited higher specific energy than the simple one implying that folding the square absorbers can raise the energy absorption. 1 and O20.3.1 adsorbers.

**5. Conclusions**

In this study, wavy square energy absorbers were investigated experimentally and numerically. The numerical studies were conducted using LS-DYNA software. The numerical results were also validated by experimental tests. The main conclusions of this study can be summarized as follows:

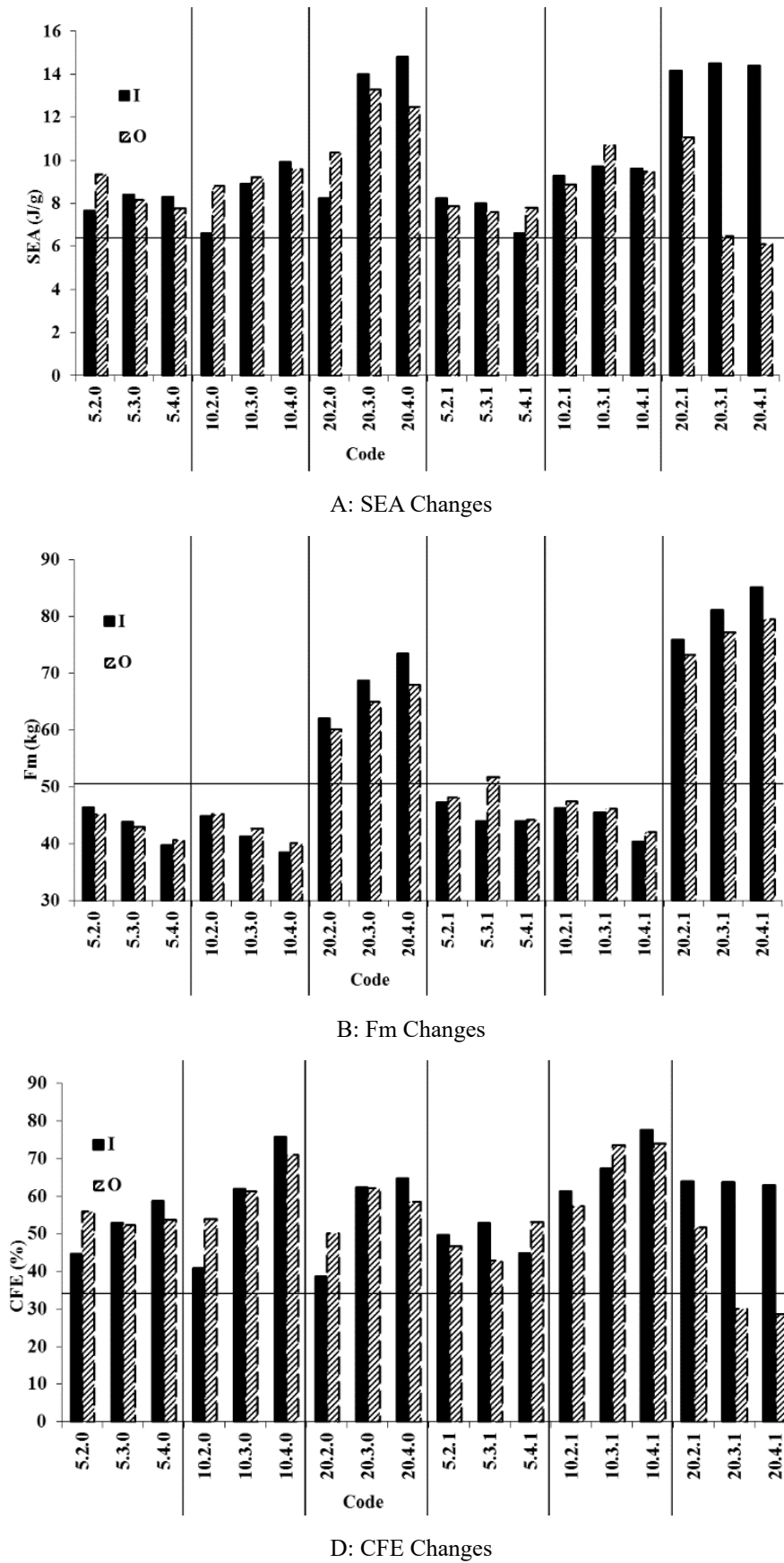


Fig. 31 The effect of internal and external half-waves on the crushing process

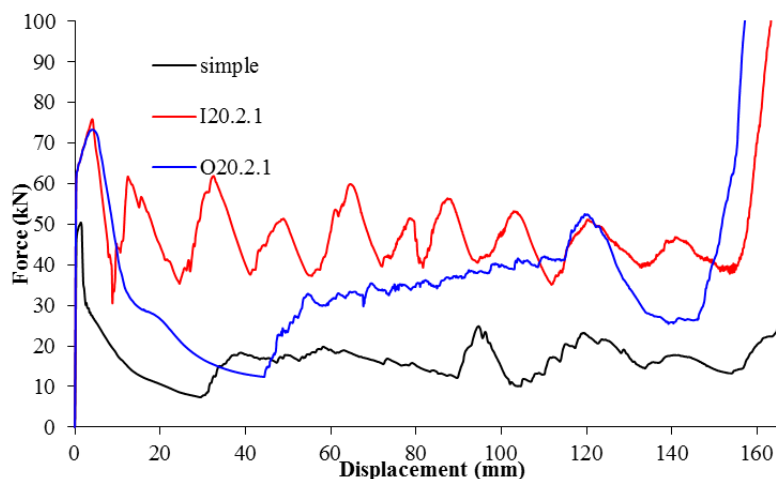


Fig. 32 The force-displacement curve of I20.2.1 and O20.2.1 absorbers

- Annealing of the aluminum shells resulted in a 76% increase in the ultimate strain and 60% and 56% decline in the yield and ultimate stresses, respectively.
- In the specimens with the half-wave height of 5 and 10 cm, an increment in the half-wave diameter reduced the maximum force; however, in specimens with a half-wave height of 20 cm, an increase in the diameter elevated the maximum force.
- In the wavy specimens, an increase in half-wave height initially declined the maximum force decreases followed by an increase.
- At constant half-wave diameter and depth, an increment of the half-wave height first improved the efficiency which was then followed by a reduction.
- Specimens with zero half-wave depth have a lower maximum force compared to those with a depth of 1 cm.
- The maximum force of the specimens with a half-wave height of 20 cm was higher than the simple ones.
- Specimens with the half-wave height of 5 and 10 cm exhibited lower maximum force compared to the simple ones.
- Folding of the square specimens often led to an augmentation in crush force efficiency.
- Concerning the specimens with a half-wave height of 20 cm, in comparison with external folding, the internal folding caused more energy absorption and higher maximum force and performance.

## References

- Abramowicz, W. (2003), "Thin-walled structures as impact energy absorbers", *Thin-Wall. Struct.*, **41**(2-3), 91-107. [https://doi.org/10.1016/S0263-8231\(02\)00082-4](https://doi.org/10.1016/S0263-8231(02)00082-4).
- Abramowicz, W. and Wierzbicki, T. (1988), "Axial crushing of foam-filled columns", *Int. J. Mech. Sci.*, [https://doi.org/10.1016/0020-7403\(88\)90059-8](https://doi.org/10.1016/0020-7403(88)90059-8).
- Abramowicz, W. and Wierzbicki, T. (1989), "Axial crushing of multicorner sheet metal columns", *J. Appl. Mech. T. ASME*, <https://doi.org/10.1115/1.3176030>.
- Abramowicz, W. (1983), "The effective crushing distance in axially compressed thin-walled metal columns", *Int. J. Impact Eng.* [https://doi.org/10.1016/0734-743X\(83\)90025-8](https://doi.org/10.1016/0734-743X(83)90025-8).
- Abramowicz, W. and Jones, N. (1984), "Dynamic axial crushing of square tubes", *Int. J. Impact Eng.* [https://doi.org/10.1016/0734-743X\(84\)90005-8](https://doi.org/10.1016/0734-743X(84)90005-8).
- Alkhatib, S.E., Tarlochan, F. and Eyvazian, A. (2017), "Collapse behavior of thin-walled corrugated tapered tubes", *Eng. Struct.*, <https://doi.org/10.1016/j.engstruct.2017.07.081>.
- ASTM Standard E8/E8M-13a. (2013), "Standard test methods for tension testing of metallic materials", *ASTM Int.*, [https://doi.org/10.1520/E0008\\_E0008M-13A](https://doi.org/10.1520/E0008_E0008M-13A).
- Bigdeli, A. and Nouri, M.D. (2019). "A crushing analysis and multi-objective optimization of thin-walled five-cell structures", *Thin-Wall. Struct.*, <https://doi.org/10.1016/j.tws.2018.12.033>.
- C. Reynolds Metals. (1958), *Aluminium Heat Treating*.
- Hanssen, A.G., Langseth, M. and Hopperstad, O.S. (2000), "Static and dynamic crushing of square aluminum extrusions with aluminum foam filler", *Int. J. Impact Eng.*, [https://doi.org/10.1016/S0734-743X\(99\)00169-4](https://doi.org/10.1016/S0734-743X(99)00169-4).
- Hanssen, A.G., Langseth, M. and Hopperstad, O.S. (2001), "Optimum design for energy absorption of square aluminum columns with aluminum foam filler", *Int. J. Mech. Sci.*, [https://doi.org/10.1016/S0020-7403\(99\)00108-3](https://doi.org/10.1016/S0020-7403(99)00108-3).
- Hayduk, R. and Wierzbicki, T. (1984). "Extensional collapse modes of structural members", *Comput. Struct.* [https://doi.org/10.1016/0045-7949\(84\)90065-8](https://doi.org/10.1016/0045-7949(84)90065-8).
- Hosseini, R., Hamed, M., Golparvar, H. and Zargar, O. (2019), "Analytical and Experimental Investigation into Increasing Operating Bandwidth of Piezoelectric Energy Harvesters", *AUT J. Mech. Eng.*, **3**(1), 113-122. <https://doi.org/10.22060/ajme.2018.14272.5718>.
- Hosseini, R., Zargar, O. and Hamed, M. (2018), "Improving power density of piezoelectric vibration-based energy scavengers", *J. Solid Mech.*, **10**(1), 98-109.
- Kiliçaslan, C. (2015), "Numerical crushing analysis of aluminum foam-filled corrugated single- and double-circular tubes subjected to axial impact loading", *Thin-Wall. Struct.* <https://doi.org/10.1016/j.tws.2015.08.009>.
- Najafi, A. and Rais-Rohani, M. (2011), "Mechanics of axial plastic collapse in multi-cell, multi-corner crush tubes", *Thin-Wall. Struct.*, <https://doi.org/10.1016/j.tws.2010.07.002>.
- Niknejad, A., Liaghat, G.H., Moslemi Naeini, H. and Behravesh, A.H. (2011), "Theoretical and experimental studies of the

- instantaneous folding force of the polyurethane foam-filled square honeycombs”, *Mater. Design.* <https://doi.org/10.1016/j.matdes.2010.06.033>.
- Niknejad, A., Liaghat, G.H., Naeini, H.M. and Behraves, A.H. (2010), “Experimental and theoretical investigation of the first fold creation in thin walled columns”, *Acta Mechanica Solida Sinica*, [https://doi.org/10.1016/S0894-9166\(10\)60036-5](https://doi.org/10.1016/S0894-9166(10)60036-5).
- Nouri Damghani, M. and Mohammadzadeh Gonabadi, A. (2016a), “Analytical and numerical study of foam-filled corrugated core sandwich panels under low velocity impact”, *Mech., Mater. Sci. Eng.*, **7**, 176-200. <https://doi.org/10.2412/mmse.6.55.34>.
- Nouri Damghani, M. and Mohammadzadeh Gonabadi, A. (2016b), “Experimental investigation of energy absorption in aluminum sandwich panels by drop hammer test. mechanics”, *Mech. Mater. Sci. Eng.*, **7**, 123-141. <https://doi.org/10.2412/mmse.6.953.525>.
- Nouri Damghani, M. and Mohammadzadeh Gonabadi, A. (2017), “Numerical and experimental study of energy absorption in aluminum corrugated core sandwich panels by drop hammer test”, *Mech. Mater. Sci. Eng.*, <https://doi.org/10.2412/mmse.85.747.458>.
- Nouri Damghani, M. and Mohammadzadeh Gonabadi, A. (2019a), “Improving the performance of the sandwich panel with the corrugated core filled with metal foam: Mathematical and Numerical methods”, *J. Mech. Adv. Compos. Struct.*, **6**(2), 249-261. <https://doi.org/10.22075/MACS.2019.15614.1171>.
- Nouri Damghani, M. and Mohammadzadeh Gonabadi, A. (2019b), “Numerical study of energy absorption in aluminum foam sandwich panel structures using drop hammer test”, *J. Sandw. Struct. Mater.*, **21**(1), 3-18. <https://doi.org/10.1177/1099636216685315>.
- Nouri Damghani, M. and Mohammadzadeh Gonabadi, A. (2019c), “Improving the Performance of the Sandwich Panel with the Corrugated Core Filled with Metal Foam: Mathematical and Numerical Methods”, *Mech. Adv. Compos. Struct.*, **6**(2), 249-261. <https://doi.org/10.22075/mac.2019.16211.1171>
- Nouri Damghani, M., Rahmani, H., Mohammadzadeh, A. and Shokri-pour, S. (2011), “Comparison of static and dynamic buckling critical force in the homogeneous and composite columns (Pillars)”, *Int. Review Mech. Eng.*, **5**(7), 1208-1212.
- Reid, S.R., Reddy, T.Y. and Gray, M.D. (1986), “Static and dynamic axial crushing of foam-filled sheet metal tubes”, *Int. J. Mech. Sci.*, [https://doi.org/10.1016/0020-7403\(86\)90043-3](https://doi.org/10.1016/0020-7403(86)90043-3).
- Reyes, A., Hopperstad, O.S. and Langseth, M. (2004), “Aluminum foam-filled extrusions Subjected to oblique loading: experimental and numerical study”, *Int. J. Solids Struct.*, <https://doi.org/10.1016/j.ijsolstr.2003.09.053>.
- Santosa, S. and Wierzbicki, T. (1998), “Crash behavior of box columns filled with aluminum honeycomb or foam”, *Comput. Struct.*, [https://doi.org/10.1016/S0045-7949\(98\)00067-4](https://doi.org/10.1016/S0045-7949(98)00067-4).
- Shahbeyk, S., Petrinic, N. and Vafai, A. (2007), “Numerical modelling of dynamically loaded metal foam-filled square columns”, *Int. J. Impact Eng.*, <https://doi.org/10.1016/j.ijimpeng.2005.11.005>.
- Shu, C., Zhao, S. and Hou, S. (2018), “Crashworthiness analysis of two-layered corrugated sandwich panels under crushing loading”, *Thin-Wall. Struct.*, <https://doi.org/10.1016/j.tws.2018.09.008>.
- Song, H.W., Fan, Z.J., Yu, G., Wang, Q.C. and Tobota, A. (2005), “Partition energy absorption of axially crushed aluminum foam-filled hat sections”, *Int. J. Solids Struct.*, <https://doi.org/10.1016/j.ijsolstr.2004.09.050>.
- Taghipoor, H. and Damghani Nouri, M. (2018), “Axial crushing and transverse bending responses of sandwich structures with lattice core”, *J. Sandw. Struct. Mater.*, 109963621876132. <https://doi.org/10.1177/1099636218761321>.
- Taghipoor, H. and Damghani Nouri, M. (2019), “Experimental and numerical investigation of lattice core sandwich beams under low-velocity bending impact”, *J. Sandw. Struct. Mater.*, **21**(6), 2154-2177. <https://doi.org/10.1177/1099636218761315>.
- Taghipoor, H. and Noori, M.D. (2018), “Experimental and numerical study on energy absorption of lattice-core sandwich beam”, *Steel Compos. Struct.*, **27**(2), 135-147. <https://doi.org/10.12989/scs.2018.27.2.135>.
- Wang, Q., Fan, Z. and Gui, L. (2007), “Theoretical analysis for axial crushing behaviour of aluminium foam-filled hat sections”, *Int. J. Mech. Sci.*, <https://doi.org/10.1016/j.ijmecsci.2006.06.011>.
- Wierzbicki, T. and Abramowicz, W. (1983), “On the crushing mechanics of thin-walled structures”, *J. Appl. Mech. T. ASME*. <https://doi.org/10.1115/1.3167137>.
- Wu, S., Li, G., Sun, G., Wu, X. and Li, Q. (2016), “Crashworthiness analysis and optimization of sinusoidal corrugation tube”, *Thin-Wall. Struct.*, <https://doi.org/10.1016/j.tws.2016.03.029>.
- Yang, M., Han, B., Su, P.B., Wei, Z.H., Zhang, Q., Zhang, Q.C., and Lu, T.J. (2019), “Axial crushing of ultralight all-metallic truncated conical sandwich shells with corrugated cores”, *Thin-Wall. Struct.*, <https://doi.org/10.1016/j.tws.2019.03.048>
- Ye, J.H., Zhao, X.L., Van Binh, D. and Al-Mahaidi, R. (2007), “Plastic mechanism analysis of fabricated square and triangular sections under axial compression”, *Thin-Wall. Struct.*, <https://doi.org/10.1016/j.tws.2007.02.006>.
- Zarei, H. and Kröger, M. (2008), “Optimum honeycomb filled crash absorber design”, *Mater. Design.* <https://doi.org/10.1016/j.matdes.2006.10.013>.
- Zarei, H.R. and Kröger, M. (2008), “Optimization of the foam-filled aluminum tubes for crush box application”, *Thin-Wall. Struct.*, <https://doi.org/10.1016/j.tws.2007.07.016>.
- Zargar, O., Masoumi, A. and Moghaddam, A.O. (2017), “Investigation and optimization for the dynamical behaviour of the vehicle structure”, *Int. J. Autom. Mech. Eng.*, **14**(2), 4196-4210. <https://doi.org/10.15282/ijame.14.2.2017.7.0336>.
- Zhang, C.J., Yi, F. and Zhang, X. (2010), “Mechanical properties and energy absorption properties of aluminum foam-filled square tubes”, *T. Nonferrous Metals Soc. China (English Edition)*, [https://doi.org/10.1016/S1003-6326\(09\)60308-3](https://doi.org/10.1016/S1003-6326(09)60308-3).
- Zhang, X. and Cheng, G. (2007), “A comparative study of energy absorption characteristics of foam-filled and multi-cell square columns”, *International Journal of Impact Engineering*. <https://doi.org/10.1016/j.ijimpeng.2006.10.007>.
- Zhang, X.W., Su, H. and Yu, T.X. (2009), “Energy absorption of an axially crushed square tube with a buckling initiator”, *Int. J. Impact Eng.*, <https://doi.org/10.1016/j.ijimpeng.2008.02.002>.
- Zhao, H. and Abdennadher, S. (2004), “On the strength enhancement under impact loading of square tubes made from rate insensitive metals”, *Int. J. Solids Struct.*, <https://doi.org/10.1016/j.ijsolstr.2004.05.039>.

CC